iScience

CellPress
OPEN ACCESS

Article

Dynamic modulation of mouse thalamocortical visual activity by salient sounds

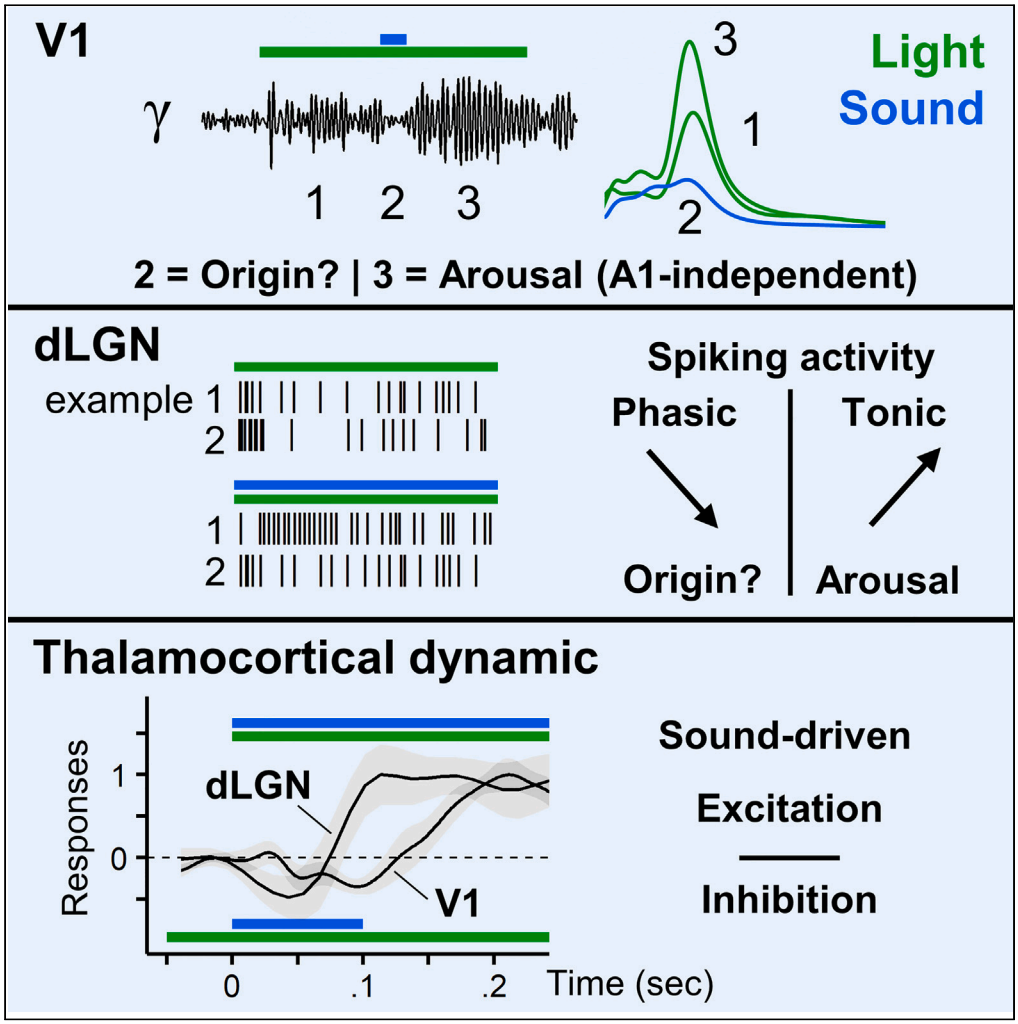

Clément E. Lemercier, Patrik Krieger, Denise Manahan-Vaughan

clement.lemercier@rub.de (C.E.L.)
denise.manahan-vaughan@rub.de (D.M.-V.)

Highlights

Sound desynchronizes and then enhances V1 gamma-band activity

Increase in V1 gamma responsiveness to sound can be explained by arousal

The visual response of the dLGN is also modulated biphasically by sound

dLGN inputs to V1 may contribute to shaping V1 visual responses to sound

Lemercier et al., iScience 27, 109364
April 19, 2024
https://doi.org/10.1016/j.isci.2024.109364

iScience

CellPress
OPEN ACCESS

Article

Dynamic modulation of mouse thalamocortical visual activity by salient sounds

Clément E. Lemercier,[1,3,*] Patrik Krieger,[1,2] and Denise Manahan-Vaughan[1,2,*]

SUMMARY

Visual responses of the primary visual cortex (V1) are altered by sound. Sound-driven behavioral arousal suggests that, in addition to direct inputs from the primary auditory cortex (A1), multiple other sources may shape V1 responses to sound. Here, we show in anesthetized mice that sound (white noise, ≥70dB) drives a biphasic modulation of V1 visually driven gamma-band activity, comprising fast-transient inhibitory and slow, prolonged excitatory (A1-independent) arousal-driven components. An analogous yet quicker modulation of the visual response also occurred earlier in the visual pathway, at the level of the dorsolateral geniculate nucleus (dLGN), where sound transiently inhibited the early phasic visual response and subsequently induced a prolonged increase in tonic spiking activity and gamma rhythmicity. Our results demonstrate that sound-driven modulations of visual activity are not exclusive to V1 and suggest that thalamocortical inputs from the dLGN to V1 contribute to shaping V1 visual response to sound.

INTRODUCTION

The brain continuously integrates inputs from multiple sensory sources to form a comprehensive and contextually rich representation of the external world. With regard to inputs to the primary sensory cortices, the perception of the primary modality can be altered by inputs from other sensory modalities.[1] This is particularly notable for the impact on visual processes of auditory inputs in the primary visual cortex (V1). Sound activates a population of V1 neurons,[2–6] influences V1 local inhibitory circuits,[2–4,7] and enhances both visual information encoding[3,5,8,9] and detection.[10–12] One well-characterized source of auditory input to V1 comprises direct projections from the primary auditory cortex (A1).[2–4,7,13,14]

In addition to the existence of this direct auditory pathway to V1, sound drives behavioral arousal, as evidenced by an increase in pupil diameter,[15,16] of respiration,[17–19] by transitions between sleep and wakefulness[20–22] and the emergence of stereotyped motor responses.[23–25] This suggests that multiple other sources could potentially contribute to V1 responsiveness to sound. Sound-driven behavioral arousal is mediated by the activation of subcortical arousal and motor circuits.[15,20–26] Such changes in behavioral state are particularly relevant in the context of visual processes, as in V1 they are associated with dynamic changes in excitability,[27] activation of a large fraction of neurons,[6,8,28,29] desynchronization of slow-wave patterns,[20–22,30] and an increase in both stimulus detection,[31,32] responsiveness,[28,32,33] and encoding.[30,34] The manifold origin of the effect of sound on V1 was recently substantiated in a report showing that sound-evoked activity in V1 can essentially be explained by the behavioral motor response to sound.[29] All this prompts questions as to the putatively diverse sources through which sound can influence V1 activity and emphasizes the need to disentangle their respective contributions in the broader context of vision.

In this study, we aimed to better identify the arousal influences of sound on V1 visual responses and investigated at the subcortical level whether these effects might be related to earlier changes in visual processes, specifically within the dorsolateral geniculate nucleus (dLGN). We recorded visually driven gamma-band (40–80 Hz) oscillations as a measure of V1 activity in the absence or presence of sound (white noise), assessed rapid effects of sound on arousal to ascertain its influence on V1 responses, and in a separate set of experiments, conducted juxtacellular recordings of dLGN neurons. To be able to disambiguate arousal-driven effects from motor-driven effects of sound, we conducted our experiments under anesthesia. In anesthetized mice, we found that sound (≥70dB) drives arousal, as indicated by an increase in the animal's respiratory rhythm and pupil diameter. Sound-driven arousal was concurrent with an increase in V1 visual gamma responsiveness independently of A1 activation. Prior to the enhancement of V1 activity, sound induced a transient desynchronization of the V1 gamma response, suggesting, in our conditions, that the effects of sound on V1 activity can be temporally and functionally decoupled into fast-onset inhibitory (whose origin remains undetermined) and slow, long-lasting (A1-independent) excitatory arousal-driven components. We observed an analogous yet quicker modulation of the visual response occurring at the level of dLGN, comprising a transient inhibition of the early phasic visual response and followed by a prolonged increase in tonic spiking activity and gamma rhythmicity. Our results demonstrate that sound-driven modulation of visual activity already occurs during the early stages of visual processing and suggest that thalamocortical inputs from the

[1]Department of Neurophysiology, Medical Faculty, Ruhr-University Bochum, 44801 Bochum, Germany
[2]Senior author
[3]Lead contact
*Correspondence: clement.lemercier@rub.de (C.E.L.), denise.manahan-vaughan@rub.de (D.M.-V.)
https://doi.org/10.1016/j.isci.2024.109364

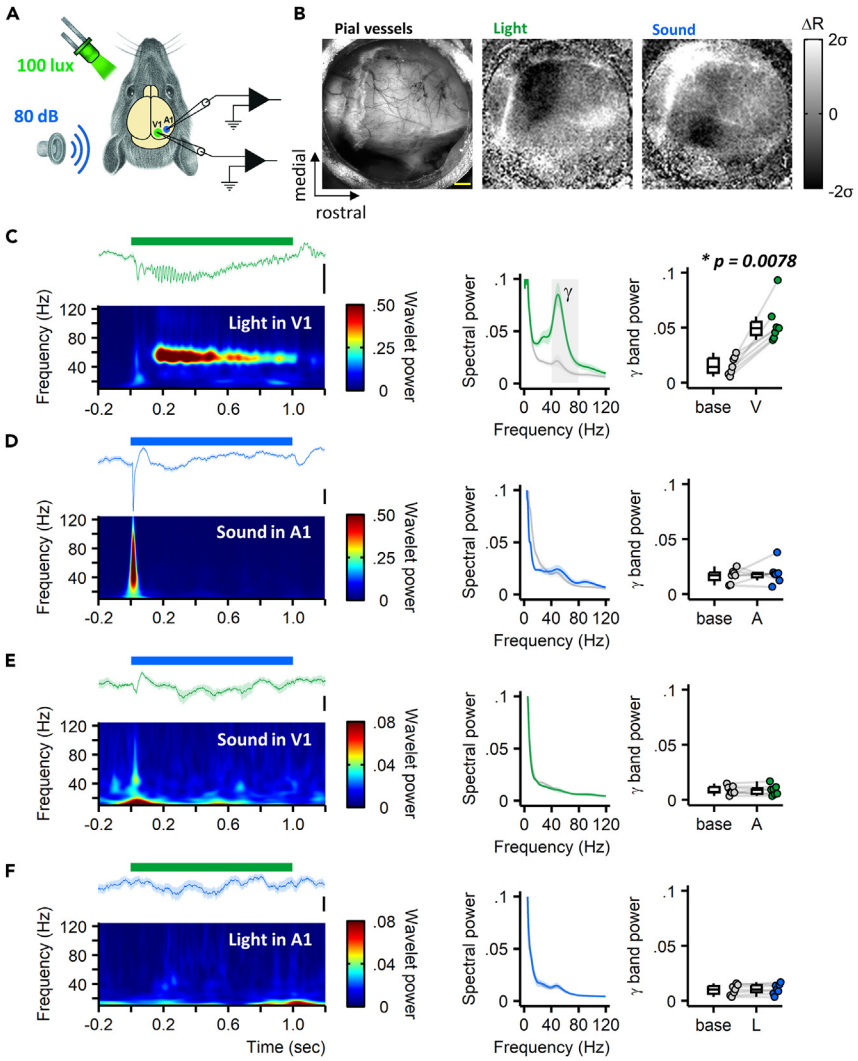

Figure 1. Sensory responses and crossmodal interactions in V1 and A1

(A) Illustration of the experimental arrangement.

(B) Example of functional delineation of V1 and A1 with IOS imaging. From left to right: background image of the skull surface and pial vessels (illuminated at 546 nm), average change (over 4 trials) in cortical light reflectance (illuminated at 630 nm) in response to visual (1 s LED flash at ~100 lux) and auditory stimuli (1 s sound at 80 dB). Frames showing the response to visual and auditory stimuli were selected 2 and 1 s following stimulus onset, respectively. Data are from the same animal; scale bar: 1 mm; scale and orientation apply to all images.

(C–F) Left: example of LFP waveforms (average of 20 trials) and corresponding wavelet power spectra showing a typical visual response in V1 (C), an auditory response in A1 (D), a sound-evoked potential in V1 (E), and the absence of crossmodal visual response in A1 (F). In (C–F), data are from the same animal; LFP scale bars: (C–D) 0.4 mV and (E–F) 0.2 mV. Right: grand average PSDs (across animals) at baseline (gray) and during sensory stimulation (colored) (N = 7), along with the quantification of gamma-band power (40–80 Hz). In boxplots, Wilcoxon signed-rank test.

dLGN to V1 might contribute to shaping V1 visual responses to sound. Sound-driven arousal, occurring even in the anesthetized state, further emphasizes the need to accurately account for alterations in animals' internal states to correctly interpret the origins of the effects of sound on visual processes.

RESULTS

Visual and auditory responses and crossmodal interactions in V1 and A1

First, we explored V1 and A1 responses to unimodal visual and auditory stimuli, by means of intracortical local field potential (LFP) recordings from layer 4 (Figures 1A and 1B). We focused on this layer because of the prominence of visual-induced gamma activity within it.[35] Given the influence of body movements on V1 activity,[6,8,28–30,32,33] recordings were carried out under anesthesia (urethane/acepromazine) to prevent

the behavioral motor response to sound. Stimulation of the visual field with a light-emitting diode induced rhythmic gamma-band (40–80 Hz) fluctuations in V1 LFP ($p = 0.0078$), with a peak frequency of 49.51 Hz (2.20) and a half-power bandwidth of 21.19 Hz (4.90) (lower edge = 40.55 Hz [4.09], upper edge = 60.29 Hz [2.26]; N = 7) (Figure 1C). In contrast to V1, the LFP power spectrum of A1 in response to white noise (80 dB SPL; white noise is thereafter referred to as sound) did not exhibit rhythmical fluctuations; rather, it consisted of "ON" and "OFF" auditory responses (Figure 1D). The initial sensory responses, comprising the visual-evoked potential (VEP) in V1 and the auditory-evoked potential (AEP) in A1, exhibited comparable amplitudes (VEP = −0.30 mV [0.25], AEP = −0.37 mV [0.44], $p = 0.6875$, N = 7; Figures S1A and S1B). Yet, AEPs in A1 showed a 2-fold faster onset compared with VEPs in V1 (VEP = 45 ms [8.5], AEP = 23 ms [3.5], $p = 0.0156$, N = 7; Figures S1A and S1B).

We then examined crossmodal sensory responses in V1 and A1. In line with earlier findings,[4] V1 exhibited a fast-onset response to sound that was visible in the LFP as a transient upward deflection (Figures 1E and S1C). In our experiments, this sound-evoked potential (SEP) in V1 had a latency, estimated at half-peak time, of 55 ms (8.7) and an amplitude of 0.13 mV (0.02) (N = 7) (Figure S1D). Although the cessation of sound triggered an "OFF" auditory response in A1 (Figure 1D), sound offset was not associated with a response in V1 (Figure S1E). In contrast to V1, A1 LFPs did not exhibit a crossmodal visual-evoked potential (Figures 1F and S1F), but rather showed a tendency towards an increase in voltage variability in the presence of visual stimulation compared with baseline (Figure S1F), suggesting a potential sensitivity of A1 LFP to visual stimuli.

Salient sounds enhance V1 gamma response independently of A1 activation

We then compared V1 gamma activity during unimodal visual (V) and bimodal audiovisual (AV) stimulation and found that V1 gamma power increased significantly when visual stimuli were combined with sound (80 dB; +64.1% [77.2], $p = 0.0078$, N = 9; Figures 2A–2C). The gamma peak frequency was unaffected in the presence of sound (V = 49.7 Hz [3.3], AV = 50.1 [6.0]; $p = 0.4412$, N = 9). The effect was immediate upon adding sound to the visual stimulus, fluctuated over the course of audiovisual trials, and then returned to baseline levels when the stimulus was switched back to visual stimulation alone; note that a few subsequent trials continued to exhibit significantly higher power (Figures S2A and S2B). Moreover, the effect was contingent on sound pressure levels, whereby a significant increase in power was observed at 80 dB ($p = 0.0078$, N = 9) and 70 dB ($p = 0.0312$, N = 7), but not at 60 dB ($p = 0.5273$, N = 8) (Figures 2B and 2C), indicating the requirement of salient sounds for this effect to occur. Notably, 60 dB sound still evoked an auditory "ON" response in A1 (Figure 2C), albeit of lower amplitude. This observation suggests that the increase in V1 gamma power to sound may not necessarily rely on A1 activation.

To test this possibility, we suppressed the A1 auditory response through either pharmacological activation of $GABA_A$ receptors using local application of muscimol ($p = 0.0156$, N = 7; Figures 2D and 2E), or by locally photo-activating channelrhodopsin in GAD2-expressing neurons ($p = 0.0312$, N = 5; Figures 2G, 2H, and S3). Under these conditions, sound continued to increase V1 gamma power (muscimol: $p = 0.0156$, N = 7; opto: $p = 0.0312$, N = 5; Figures 2F and 2I). This finding was further supported by a comparable increase in power between the control and muscimol experiments ($AV_{control}$ = +164.1% [77.2], N = 9; $AV_{muscimol}$ = +154,8% [39.2], N = 7). These results suggest that A1 activation is not required for the enhancing effect of sound on the V1 gamma response.

Enhanced V1 gamma response to sound temporally aligns with a state of elevated arousal

Changes in brain state in response to arousing stimuli, including auditory stimuli,[15,16,20–22] are conducive to the emergence of cortical gamma-band activity.[30] To ascertain a potential source of arousal contributing to the enhancing effect of sound on V1 gamma response, we examined changes in the animals' arousal state through two indicators: the pupil diameter and the respiratory rate (Figure 3). Sound triggered a reliable pupillary dilation response with a latency of ∼1 s, reaching a maximum dilation of ∼200% above baseline ∼3 s after the stimulus onset that typically exhibited a gradual return to baseline within our intertrial time interval (intertrial time interval: 10 s, trial duration: 6 s) (Figures 3A and 3B; average measurements from two experiments). The slower pupillary response to sound, as reported here, contrasts with the awake condition[15,16] and might be attributable to anesthesia.[36]

Monitoring the animal's respiration, using a piezoelectric transducer (PZT) placed beneath the chest,[37] indicated that sound (80 dB) induced a consistent, yet slight tachypneic response (i.e., rapid breathing, in the range of 3.01 Hz [0.26] to 3.24 Hz [0.42], N = 4; Figures 3C–3F), without altering the respiratory amplitude (baseline = 0.90 a.u. [0.11], A = 0.92 a.u. [0.14], N = 4). Sound-induced tachypnea has been documented elsewhere.[17–19] This momentary respiratory response was concomitant with sound presentation and ceased once sound ended (Figure 3D). The magnitude of the respiratory response linearly increased with sound pressure level (60 dB = +0.08 Hz [0.11], 70 dB = +0.26 Hz [0.12], 80 dB = +0.33 Hz [0.13], N = 3; Figure 5F), indicating similarities with the effect of sound pressure level on the V1 gamma response (Figures 2B and 2C). Contrary to sound, visual stimuli did not elicit an increase in respiration rhythm (baseline = 2.80 Hz [0.95], V = 2.80 Hz [0.90], $p = 0.1814$, N = 7; Figures 3G and 3H); however, akin to sound alone, the presence of sound along visual stimuli consistently increased the respiratory rhythm (baseline = 2.94 Hz [0.75], AV = 3.15 Hz [1.01]; $p = 0.0156$; N = 7; Figures 3G and 3H). In both cases, respiratory amplitude was unaltered (baseline = 0.72 a.u. [0.43], V = 0.77 a.u. [0.40], $p = 0.5781$, N = 7; baseline = 0.78 [0.28], AV = 0.79 a.u. [0.32], $p = 0.1563$, N = 7). The continuous monitoring of the animal's respiration through PZT signals indicated that anesthesia prevented sound from triggering body movements, implying that only thoracic respiratory movements could have been detected (trials with spontaneous body movements: V = 5%, 7/140, AV = 3.6%, 5/140 trials; N = 7). In support of this, facial images of the muscular regions of the animal's eye contour were devoid of movement. However, our imaging field did not permit us to examine the orofacial zones. These findings sugesst that, even in an anesthetized state, sound elicits a stereotyped arousal response, as evidenced here by an increase in respiratory rhythm followed by an increase in pupil size. The sound-induced increase in V1 gamma response thus appears to temporally align with an

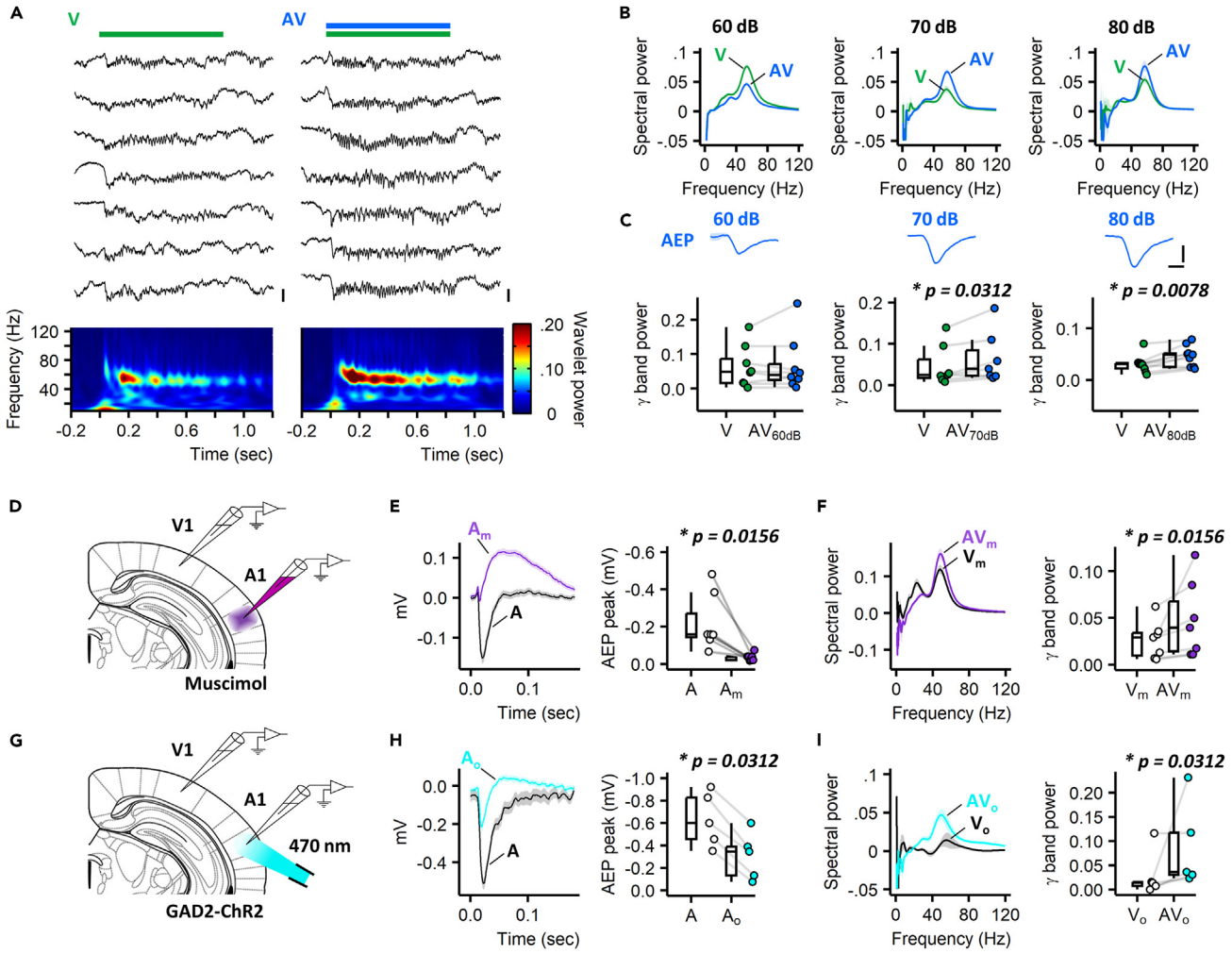

Figure 2. V1 gamma response is enhanced by salient sounds independently of A1 activation

(A) A sample of consecutively recorded V1 LFP waveforms and examples of V1 gamma responses with average wavelet power spectra during visual (V) and audiovisual stimuli (AV, 80 dB). Data are from the same animal; LFP scale bars: 0.4 mV.

(B) Example of V1 power spectral densities (PSDs) during V (green) and AV (blue) stimuli, with sound delivered at various sound pressure levels (SPLs) (spectra are selected from different experiments).

(C) Quantification of V1 gamma-band power during V and AV stimuli delivered at various SPLs (60 dB, N = 8; 70 dB, N = 7; 80 dB, N = 10). Above, examples of LFP waveforms depict A1 auditory-evoked potentials (AEPs) at the three different tested SPLs (AEPs are from the same animal; scale bars: (y) 0.2 mV and (x) 10 ms).

(D) Illustration of the experimental arrangement used for A1 inactivation experiments involving local infusion of the $GABA_A$ receptor agonist, muscimol (~1 μL at 1 mM).

(E) Left: comparison of A1 AEP before (black) and after infusion of the $GABA_A$-receptor agonist, muscimol (magenta) (average of 70 trials, N = 7). Right: quantification of A1 AEP peak amplitude before and after muscimol infusion (N = 7).

(F) Left: example of V1 PSDs during V (black) and AV (80 dB, magenta) stimuli under conditions of silenced A1 auditory responses. Right: quantification of V1 gamma-band power during V and AV stimuli under conditions of silenced A1 auditory responses (N = 7).

(G–I) Replication experiment with photo-activation of GAD2-expressing neurons in A1. Panel structure is identical to (D–F), with the cyan color representing the optogenetic condition [(H), average of 50 trials; (I), N = 5].

In (E–F) and (H–F), the lowercase letters "m" and "o," respectively, denote the muscimol and optogenetic conditions. In (C), (E–F), and (I–F), Wilcoxon signed-rank test.

elevated state of arousal. Specifically, the occurrence of sound-induced tachypnea coincided with the timing of the sound-induced increase in V1 gamma response.

Given the body of evidence on the entrainment of LFP oscillations by respiration[38] that encompass the gamma rhythm,[39–43] we then explored the relationship between respiratory rhythm and visually driven V1 gamma activity. Fluctuations in respiratory rhythm during the stimulation period, in comparison to the pre-stimulation baseline period, exhibited a positive, albeit weak, correlation with the power of the V1 gamma response both during visual or audiovisual trials (V, rho = 0.1448, p = 0.0483; AV, rho = 0.1694, p = 0.0248; Figure 3I). This

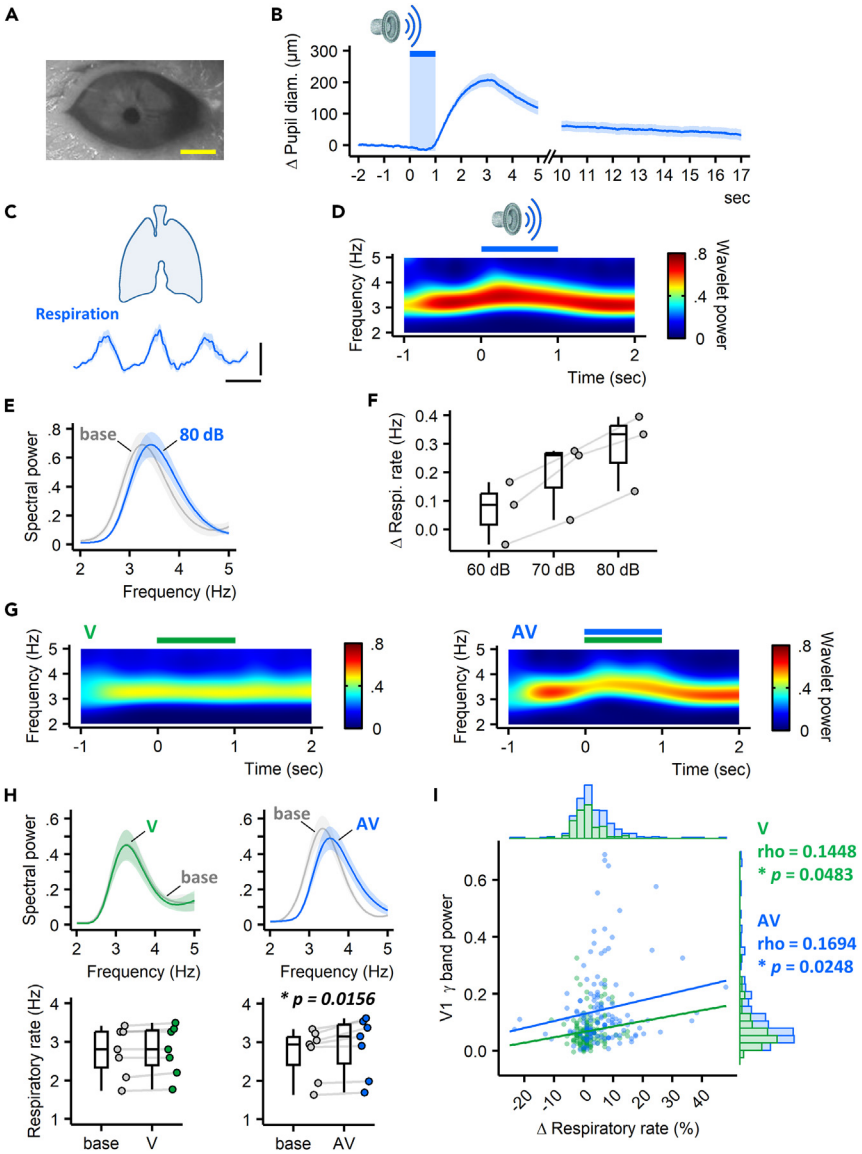

Figure 3. Enhanced V1 gamma response to sound is linked to arousal

(A) Infrared photograph of the mouse pupil (scale bar: 1 mm).

(B) Pupillary response to sound (average of 30 trials, N = 2).

(C) Example of the respiratory signal recorded with a piezoelectric transducer (PZT; average of 20 segments, phase-aligned, of the initial second preceding sound onset; scale bars: (x) 0.2 s and (y) 0.1 mV).

(D) Example of a typical wavelet spectrum of the respiratory signal (averaged over 20 trials at 80 dB), depicting the fast and transient-sound-induced tachypnea.

(E) Example of respiratory signal power spectral densities (PSDs) before (gray) and during sound (blue). Data in (D–E) are from the same experiment.

(F) Changes in respiratory rate (relative to baseline) as a function of sound pressure level (N = 3, paired observations).

(G) Example of average respiratory signal wavelet spectra during V and AV stimuli (data are from the same animal).

(H) Top: example of respiratory signal PSDs before (gray), during V (green) and AV (blue) stimuli (data from the same experiment shown in G). Bottom: quantification of the respiratory peak frequency relative to baseline (base) during V and AV stimuli (N = 7). Wilcoxon signed-rank test.

(I) Relationship between V1 gamma power and variations in respiratory rate (compared with the pre-stimulation baseline period) during V (green) and AV (blue) stimuli (V: n = 133 trials, AV: n = 135 trials; N = 7). Marginal plots depicting data histogram along the x and y axes. Colored lines represent linear regression, and rho value indicates the Spearman's rank correlation coefficient.

suggests that a faster respiratory rhythm corresponds to a stronger V1 gamma response. Although visual stimuli did not significantly impact respiration (Figures 3G and 3H), subtle inter-trial variations in the respiratory rhythm also exhibited such a relationship. Analysis of phase-amplitude coupling[44] did not reveal any obvious coupling between respiratory phase and V1 gamma amplitude (Figure S4). Analysis of

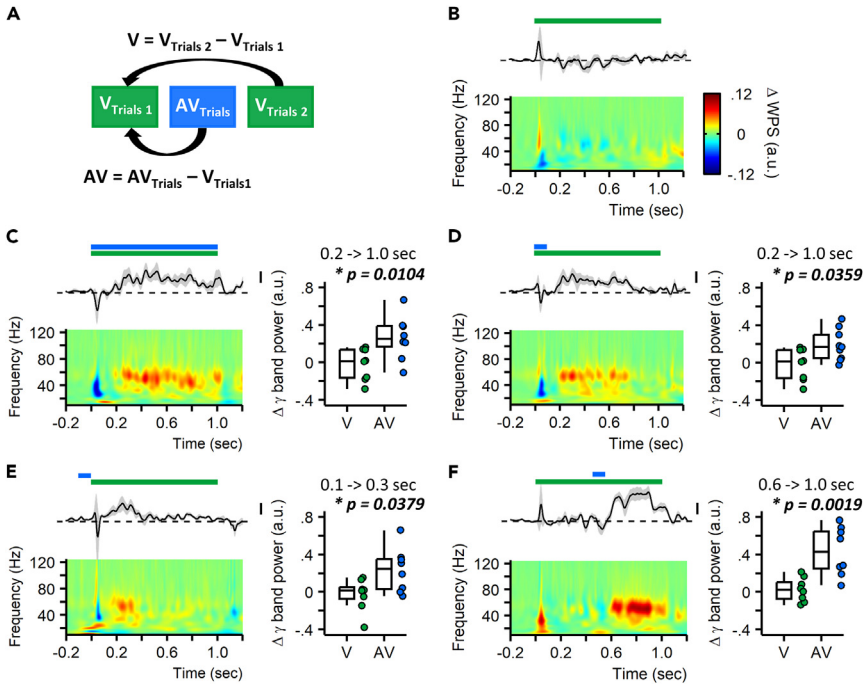

Figure 4. Sound enhances V1 gamma response regardless of when it occurs relative to the visual stimulus

(A) Illustration of the method used to compute differential wavelet power spectra (ΔWPS).

(B) Grand average (across animals) of V1 ΔWPS between two blocks of trials with visual stimuli alone (i.e., $V_{Trials\ 2}$ subtracted to $V_{Trials\ 1}$; N = 8).

(C–F) Grand average (across animals) of V1 ΔWPS (i.e., $AV_{Trials\ 2}$ subtracted to $V_{Trials\ 1}$) in response to different AV pairing. (C) Fully paired AV stimuli (N = 8); (D) partially paired AV stimuli (N = 9); (E) unpaired AV stimuli (N = 8); (F) sound delivered for 100 ms at the midpoint of visual stimulation (N = 8). In all protocols, the sound was delivered at 80 dB. The average temporal variation in V1 gamma-band power (relative to $V_{Trials\ 1}$) is depicted above each panel (shadowed area corresponds to ±SEM; scale bars in all panels: 2/100 a.u). Boxplots showing the change in V1 gamma-band power between control [V, (B)] and AV stimuli. The time ranges during which V1 gamma power significantly differs from the control are indicated above each boxplots. In (C–E), Wilcoxon-Mann-Whitney U test.

covariance (ANCOVA) confirmed the effect of respiration on V1 gamma power (R^2 = 0.1363; $F(3, 264)$ = 13.89, p = 1.946e-08) and indicated that sound increased the intercept of the linear regression model (V = 0.0663 ± 0.0096, AV = 0.1288 ± 0.0144; p = 1.9902e-05; Figure 3I) without altering its slope steepness (V = 1.901e-03 ± 2.236e-03, AV = 2.445e-03 ± 2.433e-03; p = 0.8233; Figure 3I). Sound thus appears to be associated with an enhanced level of V1 gamma power, even when fluctuations in respiratory rhythm are minimal. Moreover, the relationship between V1 gamma power and respiration appears unaltered, regardless of the presence of sound. The enhancing effect of sound on V1 gamma responses is consequently unlikely to be specifically attributed to sound-induced tachypnea. Instead, it might rely on other, as yet uncovered, aspects of sound-driven arousal, as well as on auditory responses not originating from A1.

Audiovisual congruency weakly influences V1 gamma response to sound

We then investigated the influence of the temporal coordination of visual and auditory stimuli. To this end, we implemented various stimulation paradigms, with variable sound durations and timings relative to the visual stimulation (Figure 4). Differential wavelet power spectra (Figure 4A) between two recording blocks, consisting solely of visual stimuli (N = 8; Figure 4B), were used as controls. The presentation of fully temporally synchronized auditory and visual stimuli for 1 s (i.e., our standard protocol) resulted in a sustained increase in V1 gamma power throughout the entire duration of the stimulation period (p = 0.0104, N = 8; Figure 4C). A similar increase was observed when sound was paired with visual stimuli for only 100 ms, beginning at the start of the visual stimulation (p = 0.0359, N = 9; Figure 4D). Decoupling auditory and visual stimuli, by presenting a sound for 100 ms, with a latency of 100 ms before the onset of visual stimulation, also increased the gamma power (p = 0.0379, N = 8; Figure 4E). This effect was rather transient and primarily occurred during the initial phase of the gamma response. Remarkably, delivering sound for 100 ms at the midpoint of visual stimulation led to a potent and sustained increase in gamma power (p = 0.0019, N = 8; Figure 4F). These results indicate that sound induces a prolonged increase in V1 gamma responsiveness, irrespective of its timing relative to the visual stimulus, and provide additional evidence for an arousal-based mechanism.

Sound exerts a biphasic effect on V1 gamma response

Upon delivering a sound burst of 100 ms at the midpoint of a visual stimulation (Figures 4F and 5), the subsequent increase in V1 gamma power was preceded by an SEP (Figure 5A). On average, SEPs in V1 recorded in illuminated conditions (Figure 5B) exhibited comparable

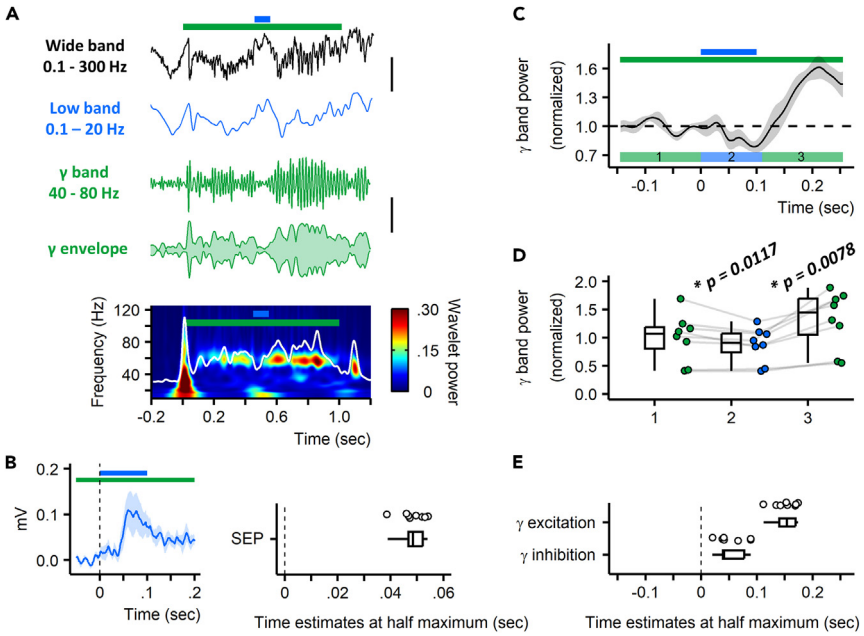

Figure 5. Sound induces a biphasic effect on V1 gamma activity

(A) Example of V1 LFP waveforms showing the wide- (0.1–300 Hz), low- (0.1–20 Hz), and gamma-band (40–80 Hz) components of the LFP and the gamma-band envelope, during presentation of brief sound (100 ms at 80 dB) delivered at the midpoint of a visual stimulation (scale bars: 0.4 and 0.2 mV). Note the emergence of a sound-evoked potential (SEP) concomitant with a decrease in gamma-band power. Below is an example of an average wavelet power spectrum with overlaid gamma-band power (white line).

(B) Left: grand average waveform of V1 SEP. Right: distribution of V1 SEP onset time measured at half maximal response (N = 8).

(C) Average gamma-band power (normalized over the 145 ms preceding sound presentation) before (1), during (2), and after (3) sound presentation (the shadowed area corresponds to ± SEM; N = 8).

(D) Quantification of V1 gamma-band power (data normalized over the 145 ms preceding sound presentation; N = 8) before (1), during (2), and after (3) sound presentation. The numbers 1–3 correspond to the time periods highlighted in (C) used for the quantification. Wilcoxon signed-rank test.

(E) Distribution of onset times (measured at half maximal response) for sound-induced gamma inhibition and excitation (N = 8).

waveforms and latencies (half-peak time estimates: 48 ms [5.5]; N = 8) compared with those recorded under dark conditions (Figures 1E, S1C, and S1D). SEPs in V1 occurred concurrently with a transient gamma desynchronization (−9.27% [32.9], p = 0.0117, N = 8; Figures 5C and 5D), indicating that, prior to exerting its enhancing effect (+44,2% [64.3], p = 0.0078, N = 8; Figures 5C and 5D), sound transiently inhibited the ongoing V1 gamma activity. Based on the time to reach half of the maximum inhibition and excitation, sound-induced inhibition and excitation of V1 gamma activity were estimated to occur 41 ms (38.5) and 154 ms (29), respectively, after sound onset (Figure 5E). Data from individual experiments are illustrated in Figure S5. The insertion of sound within the visual stimulus indicates that sound exerts a biphasic effect on ongoing visually driven V1 gamma activity, initially inducing a fast-onset transient inhibition and subsequently leading to a long-lasting excitatory response.

Biphasic visual response modulation to sound also occurs at the level of dLGN

We next sought to explore whether the effects of sound on visual activity were restricted to V1 or if such effects also occurred earlier in the anatomical hierarchy of the visual pathway. To test this possibility, we recorded juxtacellularly the visual activity of neurons in the dorsolateral geniculate nucleus (dLGN) in the absence or presence of sound (80 dB) (Figure 6). At the level of the recorded population of dLGN-ON neurons (i.e., responsive to visual stimulation onset, median recording depth: 2575 μm [372], n = 40, N = 10; Figure 6A), sound significantly increased the overall visually driven spiking activity (V = 11.77 Hz [11.46], AV = 13.02 Hz [13.92], p = 0.0017, n = 40, N = 10; Figure 6B). Notably, dLGN-ON neurons (Figure 6C) exhibited no response to sound alone (Figure 6D). At the level of individual neurons, sound had a mixed impact on their overall visual response. Specifically, 70% of the recorded neurons (n = 28) displayed an overall increased visual response of +3.5 Hz (3.3), 25% (n = 10) exhibited an overall decrease of −2.1 Hz (1.9), and 5% (n = 2) showed no change in their visual response. Data from two example neurons with opposite visual response modulation are illustrated in Figures S6A and S6B.

Visually evoked spiking patterns varied among dLGN neurons, as illustrated by individual peristimulus time histogram (PSTH) densities (Figure 6E). Most dLGN neurons exhibited an initial phasic visual response and could be subsequently distinguished based on whether or not they tonically encoded the visual stimulation period (e.g., unit 1 vs. unit 30; Figure 6E). To assess temporal variations in dLGN visual spiking patterns to sound, we computed the residual PSTH densities for each neuron between the visual and audiovisual trials (Figure 6F). Residuals revealed that sound had a dynamic influence on the visual responses of dLGN neurons. Notably, sound was not exclusively suppressive or

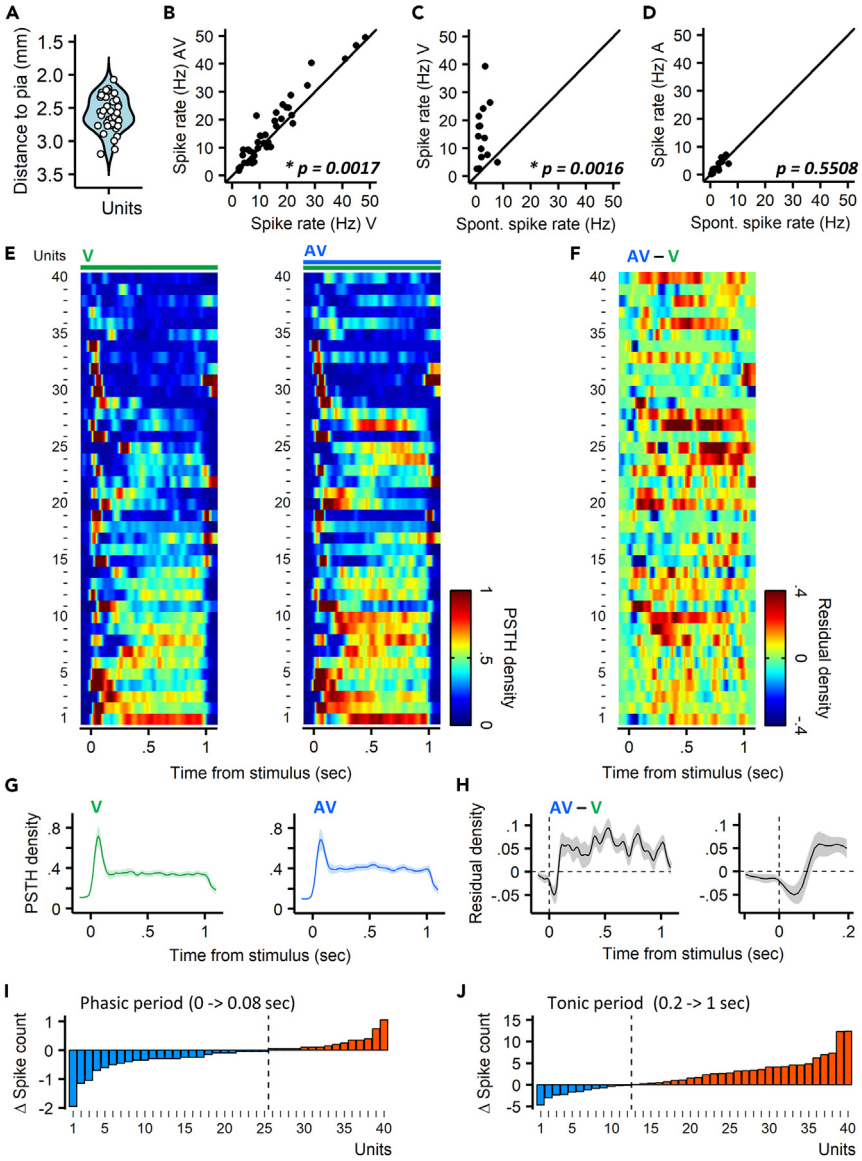

Figure 6. The visual response of the dLGN is modulated biphasically by sound

(A) Population depth distribution of the recorded dLGN-ON neurons (n = 40, N = 10).

(B) Comparison of dLGN neurons overall spike rate during V and AV stimulation (n = 40, N = 10).

(C) Comparison of dLGN neurons spike rate at baseline and during visual (V) stimulation (n = 14, N = 6).

(D) Comparison of dLGN neurons spike rate at baseline and during auditory (A) stimulation (n = 14, N = 6).

In (B–D), Wilcoxon signed-rank test.

(E) Pseudocolor plot of the dLGN neuron population's peristimulus time histogram (PSTH) density during visual (V) and audiovisual (AV) stimuli. Data are sorted in ascending order based on the overall visually induced PSTH density. The same scale applies to V and AV panels.

(F) Pseudocolor plot of the dLGN neuron population's residual PSTH density (AV subtracted to V), sorted as in (E).

(G) Grand average PSTH density during visual (V) and audiovisual (AV) stimuli (mean ± SEM).

(H) Grand average dLGN residual PSTH density (AV subtracted to V) and an enlarged view of the initial effect of sound (mean ± SEM).

(I) Average variation in spike count of the visual response of each dLGN neuron right after sound onset (0–0.08 s after sound onset).

(J) Average variation in spike count of each dLGN neuron during the continuous presence of sound (0.2–1 s).

In (I–J), downregulated and upregulated neurons are represented in blue and red, respectively.

augmentative; rather, these effects coexisted dynamically within the same neuron (e.g., unit 1, 10, and 27; Figure 6F). At the population level, the average residual density across neurons (Figures 6G and 6H) revealed, akin to V1, that the overall dLGN visual response to sound undergoes a similar biphasic modulation, comprising an initial transient inhibition followed by a prolonged excitation (Figure 6H). The

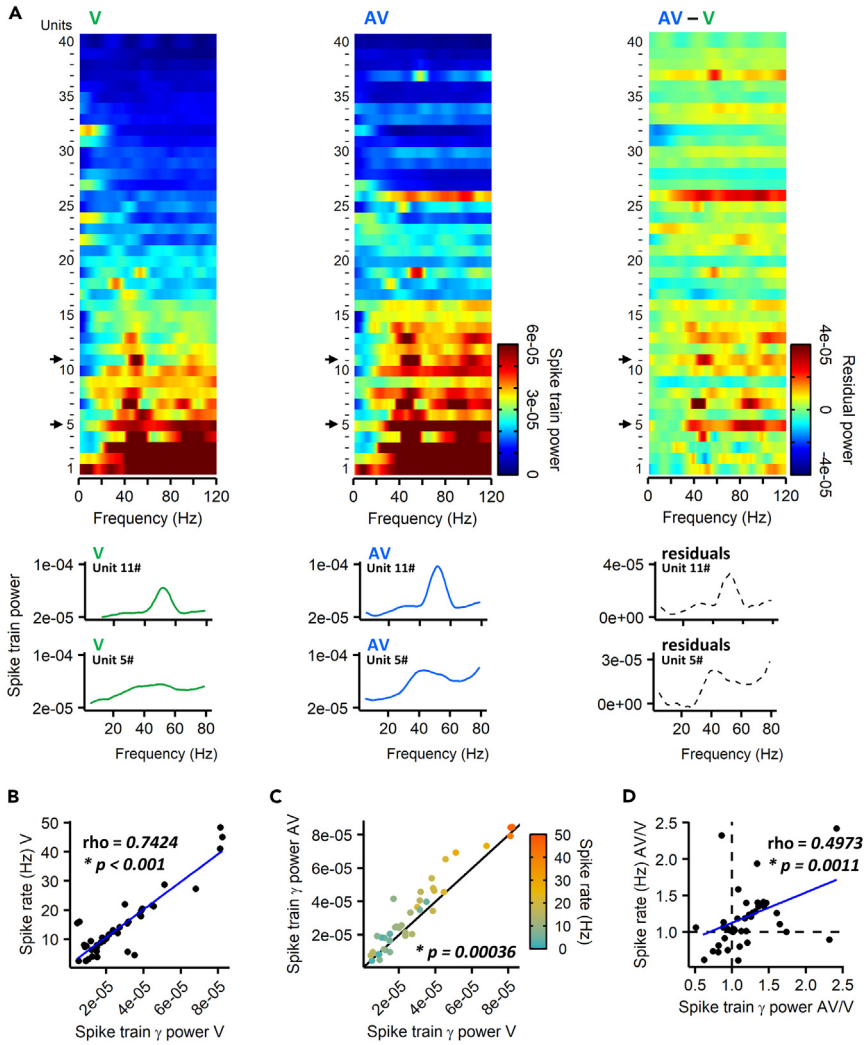

Figure 7. dLGN visual gamma-band spiking is enhanced by sound

(A) Pseudocolor plot of the dLGN neuron population's spike train power spectral densities (PSDs) (sorted in ascending order of PSD values) during visual (V, left), audiovisual condition (AV, middle), and their residuals (AV subtracted to V, right). The same scale applies to V and AV panels. Below is shown the spike train PSDs for two example neurons during V, AV stimulation, and residuals.

(B) Relationship between the spike rate of dLGN neurons and the gamma-band power of their spike trains during visual stimulation.

(C) Comparison of dLGN neurons spike train gamma-band power (40–80 Hz) during V and AV stimuli; the color code represents the spike rate of individual neurons during visual stimulation. Wilcoxon signed-rank test.

(D) Relationship between the AV-induced variation in spike train gamma-band power and spike rate.

In (B and D), the blue line corresponds to the linear regression, and rho is the value of the Spearman's rank correlation coefficient.

suppressive effect of sound was particularly prominent during the onset phase of the visual response (i.e., 0–0.08 s after stimulus onset) where most neurons exhibited phasic spiking activity. Among the subset of downregulated neurons (62.5%, n = 25, Figure 6I), the median spike rate suppression was −3.7 Hz (4.4) (Figure 6I). In the subsequent phase of the visual stimulation (i.e., from 0.2 to 1 s after stimulus onset), during which most neurons engaged in tonic spiking activity, the effect of sound was mainly excitatory. Among the subset of upregulated neurons (67.5%, n = 27, Figure 6J), the median spike rate augmentation was +4.0 Hz (3.9) (Figure 6J).

Sound enhances dLGN visual gamma-band spiking

Given the contribution of the dLGN to the emergence of V1 gamma activity,[45–47] we next examined whether the excitatory influences of sound on dLGN visual responses were also concomitant with a change in gamma-band spiking activity. Spectral analysis of the entire visually evoked spike train indicated that ~50% of the recorded dLGN neurons exhibited rhythmic spiking activity within the gamma frequency band (Figure 7A). The degree of tuning ranged from broadband to narrowband gamma (e.g., unit 5 vs. unit 11; Figure 7A). The spiking gamma-band

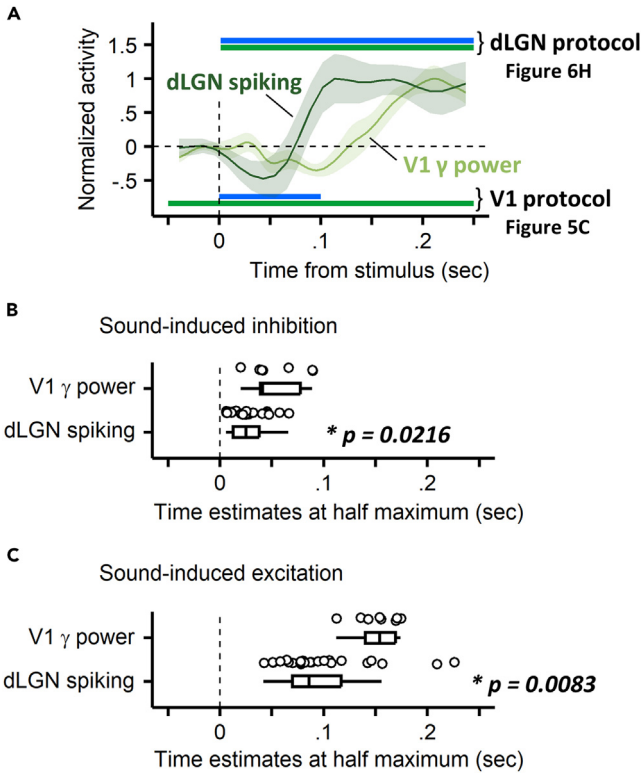

Figure 8. dLGN exhibits quicker biphasic response dynamics to sound compared to V1

(A) Overlay of the biphasic visual response modulation to sound in V1 and dLGN (V1: N = 8, data from Figure 5C; dLGN: n = 40, N = 10, data from Figure 6H). Data are aligned to sound onset and normalized based on the maximal increase.

(B) Comparison of the timing of sound-induced V1 gamma and dLGN spiking inhibition (V1: N = 8; dLGN: n = 22).

(C) Comparison of the timing of sound-induced V1 gamma and dLGN spiking excitation (V1: N = 8; dLGN: n = 26).

In (B–C), Wilcoxon-Mann-Whitney U test.

power (40–80 Hz) strongly correlated with the neurons' spike rate (Rho = 0.7424, $p < 0.001$; Figure 7B). Comparison between the spiking gamma-band power in the absence or presence of sound indicated that sound increased the gamma power of the majority of neurons that exhibited rhythmic gamma-band spiking ($p = 0.0003$; Figure 7C). The enhancing effect of sound on dLGN gamma spiking activity was also visible in the power spectral density residuals of individual neurons between the audiovisual and visual trials (Figure 7A). Sound-induced changes in both dLGN spike rate and gamma power exhibited a positive covariance (Rho = 0.4973, $p = 0.0011$; Figure 7D), indicating that spike rate variations to sound are likely to be accompanied by corresponding variations in gamma power and *vice versa*. These results indicate that, in addition to increasing the overall spiking activity of dLGN neurons, sound also enhances their spiking gamma rhythmicity.

Sound-driven biphasic visual response is quicker in the dLGN than in V1

Given the notable similarities in the biphasic effect of sound at both thalamic and cortical levels, that were initially suppressive and then augmentative, we proceeded to compare their respective dynamics by creating an overlay of V1 and dLGN visual responses to sound (Figure 8A). This comparison suggested that both sound-induced inhibition and excitation occurred with faster dynamics in the dLGN than in V1. To confirm this effect, we assessed the timing of the biphasic response in the dLGN by calculating the time to reach half-maximal suppression or augmentation using PSTH densities from the population of downregulated (Figure 6I) and upregulated neurons (Figure 6J) and compared the results with V1 gamma inhibition/excitation time estimates (i.e., from the Figure 5E). This comparison confirmed that both sound-induced inhibition (dLGN = 25 ms [25], n = 22, V1 = 41 ms [38], N = 8, $p = 0.0216$; Figure 8B) and excitation (dLGN = 87 ms [64], n = 26, V1 = 154 ms [29], N = 8, $p = 0.0083$; Figure 8C) occurred with shorter latencies in the dLGN than in V1.

DISCUSSION

Our results reveal that salient sounds (white noise, ≥70dB) drive a biphasic modulation of the thalamocortical visual response in anesthetized mice and demonstrate that sound-driven modulation of visual activity is not exclusive to V1, but also occurs at the level of the dLGN. Given the resemblance but nonetheless faster dynamics of the dLGN visual response to sound compared with V1, we propose that feedforward thalamocortical inputs from dLGN to V1 might contribute to shaping V1 visual response to sound. More generally, in our conditions, we propose,

that the effects of sound on V1 visual activity can be temporally and functionally decoupled into fast-onset inhibitory (whose origin remains undetermined) and slow, long-lasting (A1-independent) excitatory arousal-driven components. The present study complements current research efforts aimed at disentangling the multiple sources through which sound modulates visual processes.[8,29,48]

Distinct pathways are likely to mediate the biphasic effects of sound on V1

The characteristics of the enhanced V1 gamma responsiveness to sound, as reported here, favor an arousal-based origin. The effects required loud sound intensities of at least 70 dB, did not require specific audiovisual congruency, exhibited a relatively late onset to sound (~150 ms), persisted over time, even in the absence of sound, and occurred concomitantly with an elevated state of arousal, as evidenced by an increase in the animal's respiratory rhythm. Moreover, we found that this effect was independent of A1 activation. The use of anesthetics suppressed the stereotyped behavioral motor response to sound, but failed to prevent sound-driven arousal. That said, we did not conduct causal testing to investigate the role of A1 in the genesis of the animal's arousal response. A possible explanation for the non-requirement of A1, in the effect we report here, could involve the activation of subcortical ascending neuromodulatory circuits of the locus coeruleus (LC) and the basal forebrain (BF) to sound.[15,20,21] Indeed, stimulation of the LC or BF triggers a generalized arousal response,[15,20,21,26,49–51] reproducing many of the same effects as those we report in response to sound, including an increase in pupil size,[15,20,51] respiratory rhythm,[52] and cortical gamma-band activity.[53–55] Additionally, the amplitude of the visual gamma response showed a tendency to stay elevated following a block of repeated audiovisual trials, suggesting the maintenance of high arousal levels or, alternatively, a stimulus-based repetition effect.[56] The inferior colliculus, a midbrain region of the ascending auditory pathway, has been proposed by others to "serve as anatomical substrate that couples audition and arousal."[22] More generally, we anticipate that analogous effects in V1 may occur in response to arousing stimuli from other sensory modalities. Furthermore, sound-related effects on arousal are not expected to be specific to V1 and are anticipated to also occur in other sensory cortices, although the direction of these effects may vary depending on the modality.[27]

Sound alone did not trigger a gamma response in V1. Instead, it elicited an SEP in this region. During visual stimulation, V1 SEP preceded sound-driven arousal and was temporally aligned with a transient desynchronization of V1 gamma response. The SEP in V1 was described as reflecting hyperpolarization of V1 L2/3 pyramidal neurons that occurs upon activation of corticocortical connections from A1 to V1.[4] Although we did not conduct causal experiments involving the manipulation of A1 activity, one could argue that the sound-induced inhibition of V1 gamma activity reported here may involve this same pathway. Indeed, several reports have attributed the inhibitory effect of sound on V1 activity to direct auditory inputs from A1 to V1.[2–4,7] Moreover, the onset latency of sound-induced inhibition of V1 gamma (~41 ms) that we detected was comparable with that of sound-induced V1 hyperpolarization reported by others (~36 ms).[4] Hence, replicating the experiments is essential to definitively assess the role of A1 in this phenomenon and, more broadly, to determine whether or not transient V1 gamma desynchronization represents a purely auditory phenomenon. Another question that arises pertains to the putative links existing between the modulation of V1 visual response to sound and the effects of sound on dLGN visual response.

Influences of sound on dLGN visual responses

Few studies have documented crossmodal sensory modulation occurring at the level of first-order thalamic nuclei.[57–59] Here, we show that sound drives a biphasic modulation of the dLGN visual response, in the absence of a monomodal dLGN response to auditory stimuli alone. The use of high-throughput recording methods is, however, recommended to clearly ascertain the influence of sound alone on dLGN activity. Modulation of dLGN visual responses to sound comprised an initial fast-onset transient inhibition of the early phasic visual response, followed by a prolonged increase in tonic spiking activity and gamma rhythmicity. The inhibitory and excitatory effects of sound were not restricted to phasic or tonic responsive neurons but rather coexisted within the same neurons. This suggests that sound may influence targets that provide global inhibition and excitation to dLGN. Interestingly, a human fMRI study has also reported that sound increases the LGN visual response and indicated that this effect occurred along with an increased LGN/V1 interregional coupling and enhanced V1 responsiveness to low-intensity visual stimuli.[60] Whether the enhancing effect of sound on dLGN activity is contingent on arousal levels remains an open question, as arousal measures were not conducted during our dLGN recordings. Yet, under equivalent experimental conditions, we detected rapid changes in arousal following sound presentation, suggesting that this may be the case. Furthermore, several aspects of our findings and reports by others seem to favor an arousal-based mechanism: (1) we did not detect auditory response in the dLGN; (2) activation of neuromodulatory arousal circuitry upregulates its activity;[61] (3) dLGN activity, including gamma activity, is influenced by arousal;[62,63] (4) arousal modulates visual processes at all stages along the visual pathway, as evidenced by the modulation of retinal axons projecting to the dLGN and superior colliculus.[64,65] Additional investigations are required to explore the circuitry behind the sound-induced fast transient inhibition of dLGN phasic visual response. The most pressing experiment would entail recording the dLGN visual response to sound while manipulating A1 activity, as this effect could involve the modulation of subcortical circuits through descending A1 corticofugal projections.[23,24] In line with this hypothesis, it has been recently shown that corticofugal projections from the primary somatosensory cortex (S1) mediate suppression of A1 auditory response to whisker deflection through subcortical inhibition of the auditory thalamic nuclei.[66] Whether a similar circuit mechanism might underlie the suppressive effect of sound on dLGN visual response remains to be explored.

On the thalamic origins of the cortical effects of sound

All of this raises the question as to how the effects of sound originate within the visual thalamocortical circuit and as whether these effects propagate from the dLGN to V1 in a feedforward manner or *vice versa* from V1 to dLGN through corticothalamic feedback. Although our

dLGN experiments were not conducted using a protocol that allowed us to identify the biphasic effect of sound on V1 gamma activity, we also observed a remarkable, yet quicker, biphasic sound-driven modulation of the dLGN visual response. The quicker dynamics observed in the dLGN raise the intriguing possibility that sound-induced effects in V1 might originate first in the dLGN and then be relayed in V1 through feedforward corticothalamic inputs from the dLGN. Visual gamma activity, particularly driven by stimuli devoid of contrast, such as those used in the present study, delivered with a light-emitting diode, exhibits narrowband spectral features.[46] At the level of V1, narrowband gamma activity is thought to originate in a feedforward manner from dLGN inputs[45–47] that probably derives from upstream retinal inputs.[67,68] From the mechanistic standpoint of narrowband gamma activity, one could argue that the excitatory effect of sound on V1 gamma responsiveness stems from the dLGN, or even earlier, and subsequently propagates to V1. The thalamocortical hypothesis of sound-induced increase in V1 response gains additional support from a recent study, showing that corticothalamic feedback weakly contributes to the influence of behavioral states on dLGN activity.[69] Continuing with this hypothesis, the arousal-related effects of sound may be linked to changes in thalamic reticular nucleus activity,[70] which gates thalamocortical communication[71,72] and serves as a strong modulator of dLGN/V1 gamma activity.[73] Although the aforementioned elements revolve around the potential contribution of the dLGN to sound-induced increase of V1 gamma activity, the sensitivity of dLGN tonic activity to sound onset was not investigated in the present study. Hypothesizing that sound onset could lead to a reduction of dLGN tonic spiking, the opposite effect (i.e., the sound-induced transient V1 gamma desynchronization) could, in principle, also rely on reduced dLGN activity. Experiments involving simultaneous recordings from dLGN/V1 will provide valuable information for a more accurate characterization of the directionality of sound-driven biphasic modulation of thalamocortical visual activity.

Functional implications

At the functional level, the bimodal effect of sound on visual processes appears to resemble a reactive mechanism that could serve to optimize the detection and responsiveness to environmental changes or potential threats. On the one hand, the transient suppression of visual activity by sound may serve to promote momentary prioritization of unexpected sound stimuli (as suggested by others),[4] implying a shift in attention to potential sources of danger. On the other hand, the subsequent increase in arousal and visual responsiveness may reflect an adaptive response to salient sensory cues, thereby enhancing the overall readiness required for fast behavioral responses. Consistent with this interpretation, we suggest that the increase in visual responsiveness through sound-driven arousal might contribute to the reported effect of sound on visual information encoding[3,5,8,9] and detection.[10–12]

Contribution of respiration/arousal to V1 gamma activity

We detected a delayed increase in pupil diameter following sound presentation, which was initiated after the V1 visual response. Although pupil diameter is generally favored over respiration as a general indicator of arousal, most likely due to its well-established association with internal states,[15,16,20,51] our results, obtained under anesthesia, seem to suggest that respiration might represent an earlier biomarker of arousal than changes in pupil diameter. Monitoring of the animal's respiration through thoracic movements enabled us to highlight a potential connection between respiratory rhythm and the magnitude of the visual gamma response in V1. Mounting evidence supports a coupling between respiration and gamma-band oscillations.[38–43] Specifically, in V1, the membrane potential of neurons exhibit respiration-like rhythmical fluctuations[74] and the amplitude of spontaneous gamma activity phase-locks with the respiratory cycle,[39,42] indicating that V1 can indeed carry signals related to respiration. We identified a positive covariation between fluctuations in respiratory rhythm and the power of visually-driven V1 gamma activity. Although statistically weak, the presence of this correlation in both visual and audiovisual trials strengthen its validity. This correlation occurred without obvious phase-amplitude coupling between respiration phase and gamma amplitude, suggesting that this feature might be specific to spontaneous gamma activity.[39,42] However, the relationship between the visual gamma response and respiration might not be specific to the latter, as other markers of arousal could also exhibit such a relationship. Fluctuations in the magnitude of the visual gamma response might, thus, be solely linked to the overall arousal state. Future investigations on this matter could yield exciting insights on the contribution of respiration to visual processes and more broadly on the dynamic interplay between respiration and arousal.[75]

Limitations of the study

Our study did not include random stimulus presentations, but instead used blocks of repeated stimuli of the same modality. Moreover, electrophysiological signals were monitored in "sweep" mode with unmonitored intertrial periods. On the one hand, these limitations hindered us from investigating lasting arousal-related changes to sound, such as alterations in cortical state through slow-wave desynchronization.[76] On the other hand, given that urethane anesthesia is characterized by cyclical alternations of brain state,[77] this may have introduced a bias due to the potential distortion of visual responses recorded across different brain states. Intricately linked to arousal, it should be noted that sound-induced tachypnoea is inherently associated with an unintentional motor component through an increase in the frequency of thoracic respiratory movements. This motor effect could be regarded as an additional factor contributing to the effects of sound on visual activity. Although our data suggest that anesthesia effectively prevented the behavioral motor responses to sound, it must be noted that the biphasic effect of sound on the dLGN visual response demonstrates interesting parallels with the effects of saccadic eye movements, including similar dynamics.[78] Although others have reported in awake mice that salient sounds induce saccades,[2] our measurements of the animal's eye under anesthesia did not show any evidence of sound-induced oculomotor movement. However, our measures were based on a limited number of observations, and, as a result, the potential contribution of saccadic eye movements in the effects we report cannot be entirely ruled out.

STAR★METHODS

Detailed methods are provided in the online version of this paper and include the following:

- KEY RESOURCES TABLE
- RESOURCE AVAILABILITY
  - Lead contact
  - Materials availability
  - Data and code availability
- EXPERIMENTAL MODEL AND STUDY PARTICIPANT DETAILS
  - Animals
- METHOD DETAILS
  - Surgical procedures
  - Imaging of intrinsic optical signals
  - Sensory stimulation
  - Electrophysiological recordings
  - Ligand infusion
  - Optogenetic stimulation
  - Imaging of the pupil
  - Monitoring of respiration and body movement
  - Recording protocol
- QUANTIFICATION AND STATISTICAL ANALYSIS
  - Quantification of sensory-evoked potentials
  - Spectral analysis of local field potentials
  - Analysis of single-unit activity
  - Spectral analysis of respiratory signals
  - Phase-amplitude coupling analysis
  - Statistics

SUPPLEMENTAL INFORMATION

Supplemental information can be found online at https://doi.org/10.1016/j.isci.2024.109364.

ACKNOWLEDGMENTS

This research was funded by grants from the Deutsche Forschungsgemeinschaft (DFG, German Research Foundation, www.dfg.de), SFB 874/A9 & B1 - project number: 122679504 to P.K. and D.M.-V.; SPP 2411 - project number: 520284247 to D.M.-V.

We thank Ann-Christin Ammann and Josephine Ansorge for technical support and Katja Reinhard (SISSA, Italy) for helpful discussions. We also thank the five anonymous reviewers for their valuable comments on earlier versions of this paper.

AUTHOR CONTRIBUTIONS

Conceptualization, C.E.L., P.K., and D.M.-V.; methodology, C.E.L.; investigation, C.E.L.; formal analysis, C.E.L.; visualization, C.E.L.; writing—original draft, C.E.L. and D.M.-V.; writing—review & editing, C.E.L. and D.M.-V.; funding acquisition, P.K. and D.M.-V.

DECLARATION OF INTERESTS

The authors declare no competing interests.

Received: June 9, 2023
Revised: December 11, 2023
Accepted: February 26, 2024
Published: February 29, 2024

REFERENCES

1. Ghazanfar, A.A., and Schroeder, C.E. (2006). Is neocortex essentially multisensory? Trends Cogn. Sci. *10*, 278–285. https://doi.org/10.1016/j.tics.2006.04.008.
2. Deneux, T., Harrell, E.R., Kempf, A., Ceballo, S., Filipchuk, A., and Bathellier, B. (2019). Context-dependent signaling of coincident auditory and visual events in primary visual cortex. Elife *8*, e44006. https://doi.org/10.7554/eLife.44006.
3. Ibrahim, L.A., Mesik, L., Ji, X.Y., Fang, Q., Li, H.F., Li, Y.T., Zingg, B., Zhang, L.I., and Tao, H.W. (2016). Cross-Modality Sharpening of Visual Cortical Processing through Layer-1-Mediated Inhibition and Disinhibition. Neuron *89*, 1031–1045. https://doi.org/10.1016/j.neuron.2016.01.027.
4. Iurilli, G., Ghezzi, D., Olcese, U., Lassi, G., Nazzaro, C., Tonini, R., Tucci, V., Benfenati, F., and Medini, P. (2012). Sound-Driven Synaptic

Inhibition in Primary Visual Cortex. Neuron *73*, 814–828. https://doi.org/10.1016/j.neuron.2011.12.026.

5. Meijer, G.T., Montijn, J.S., Pennartz, C.M.A., and Lansink, C.S. (2017). Audiovisual Modulation in Mouse Primary Visual Cortex Depends on Cross-Modal Stimulus Configuration and Congruency. J. Neurosci. *37*, 8783–8796. https://doi.org/10.1523/JNEUROSCI.0468-17.2017.
6. Mesik, L., Huang, J.J., Zhang, L.I., and Tao, H.W. (2019). Sensory- and Motor-Related Responses of Layer 1 Neurons in the Mouse Visual Cortex. J. Neurosci. *39*, 10060–10070. https://doi.org/10.1523/JNEUROSCI.1722-19.2019.
7. Garner, A.R., and Keller, G.B. (2022). A cortical circuit for audio-visual predictions. Nat. Neurosci. *25*, 98–105. https://doi.org/10.1038/s41593-021-00974-7.
8. Williams, A.M., Angeloni, C.F., and Geffen, M.N. (2023). Sound improves neuronal encoding of visual stimuli in mouse primary visual cortex. J. Neurosci. *43*, 2885–2906. https://doi.org/10.1523/JNEUROSCI.2444-21.2023.
9. McClure, J.P., and Polack, P.-O. (2019). Pure tones modulate the representation of orientation and direction in the primary visual cortex. J. Neurophysiol. *121*, 2202–2214. https://doi.org/10.1152/jn.00069.2019.
10. Gleiss, S., and Kayser, C. (2012). Audio-Visual Detection Benefits in the Rat. PLoS One *7*, e45677. https://doi.org/10.1371/journal.pone.0045677.
11. Meijer, G.T., Pie, J.L., Dolman, T.L., Pennartz, C.M.A., and Lansink, C.S. (2018). Audiovisual Integration Enhances Stimulus Detection Performance in Mice. Front. Behav. Neurosci. *12*, 231. https://doi.org/10.3389/fnbeh.2018.00231.
12. Meijer, G.T., Marchesi, P., Mejias, J.F., Montijn, J.S., Lansink, C.S., and Pennartz, C.M.A. (2020). Neural Correlates of Multisensory Detection Behavior: Comparison of Primary and Higher-Order Visual Cortex. Cell Rep. *31*, 107636. https://doi.org/10.1016/j.celrep.2020.107636.
13. Majka, P., Rosa, M.G.P., Bai, S., Chan, J.M., Huo, B.-X., Jermakow, N., Lin, M.K., Takahashi, Y.S., Wolkowicz, I.H., Worthy, K.H., et al. (2019). Unidirectional monosynaptic connections from auditory areas to the primary visual cortex in the marmoset monkey. Brain Struct. Funct. *224*, 111–131. https://doi.org/10.1007/s00429-018-1764-4.
14. Meijer, G.T., Mertens, P.E.C., Pennartz, C.M.A., Olcese, U., and Lansink, C.S. (2019). The circuit architecture of cortical multisensory processing: Distinct functions jointly operating within a common anatomical network. Prog. Neurobiol. *174*, 1–15. https://doi.org/10.1016/j.pneurobio.2019.01.004.
15. Breton-Provencher, V., and Sur, M. (2019). Active control of arousal by a locus coeruleus GABAergic circuit. Nat. Neurosci. *22*, 218–228. https://doi.org/10.1038/s41593-018-0305-z.
16. Montes-Lourido, P., Kar, M., Kumbam, I., and Sadagopan, S. (2021). Pupillometry as a reliable metric of auditory detection and discrimination across diverse stimulus paradigms in animal models. Sci. Rep. *11*, 3108. https://doi.org/10.1038/s41598-021-82340-y.
17. Bondarenko, E., Hodgson, D.M., and Nalivaiko, E. (2014). Amygdala mediates respiratory responses to sudden arousing stimuli and to restraint stress in rats. Am. J. Physiol. Regul. Integr. Comp. Physiol. *306*, R951–R959. https://doi.org/10.1152/ajpregu.00528.2013.
18. Gomez, P., and Danuser, B. (2004). Affective and physiological responses to environmental noises and music. Int. J. Psychophysiol. *53*, 91–103. https://doi.org/10.1016/j.ijpsycho.2004.02.002.
19. Kabir, M.M., Beig, M.I., Baumert, M., Trombini, M., Mastorci, F., Sgoifo, A., Walker, F.R., Day, T.A., and Nalivaiko, E. (2010). Respiratory pattern in awake rats: Effects of motor activity and of alerting stimuli. Physiol. Behav. *101*, 22–31. https://doi.org/10.1016/j.physbeh.2010.04.004.
20. Hayat, H., Regev, N., Matosevich, N., Sales, A., Paredes-Rodriguez, E., Krom, A.J., Bergman, L., Li, Y., Lavigne, M., Kremer, E.J., et al. (2020). Locus coeruleus norepinephrine activity mediates sensory-evoked awakenings from sleep. Sci. Adv. *6*, eaaz4232. https://doi.org/10.1126/sciadv.aaz4232.
21. McKenna, J.T., Thankachan, S., Uygun, D.S., Shukla, C., McNally, J.M., Schiffino, F.L., Cordeira, J., Katsuki, F., Zant, J.C., Gamble, M.C., et al. (2020). Basal Forebrain Parvalbumin Neurons Mediate Arousals from Sleep Induced by Hypercarbia or Auditory Stimuli. Curr. Biol. *30*, 2379–2385.e4. https://doi.org/10.1016/j.cub.2020.04.029.
22. Shin, A., Park, S., Shin, W., Woo, J., Jeong, M., Kim, J., and Kim, D. (2023). A brainstem-to-mediodorsal thalamic pathway mediates sound-induced arousal from slow-wave sleep. Curr. Biol. *33*, 875–885.e5. https://doi.org/10.1016/j.cub.2023.01.033.
23. Li, Z., Wei, J.-X., Zhang, G.-W., Huang, J.J., Zingg, B., Wang, X., Tao, H.W., and Zhang, L.I. (2021). Corticostriatal control of defense behavior in mice induced by auditory looming cues. Nat. Commun. *12*, 1040. https://doi.org/10.1038/s41467-021-21248-7.
24. Xiong, X.R., Liang, F., Zingg, B., Ji, X.y., Ibrahim, L.A., Tao, H.W., and Zhang, L.I. (2015). Auditory cortex controls sound-driven innate defense behaviour through corticofugal projections to inferior colliculus. Nat. Commun. *6*, 7224. https://doi.org/10.1038/ncomms8224.
25. Yeomans, J.S., and Frankland, P.W. (1995). The acoustic startle reflex: neurons and connections. Brain Res. Rev. *21*, 301–314. https://doi.org/10.1016/0165-0173(96)00004-5.
26. Maness, E.B., Burk, J.A., McKenna, J.T., Schiffino, F.L., Strecker, R.E., and McCoy, J.G. (2022). Role of the locus coeruleus and basal forebrain in arousal and attention. Brain Res. Bull. *188*, 47–58. https://doi.org/10.1016/j.brainresbull.2022.07.014.
27. Shimaoka, D., Harris, K.D., and Carandini, M. (2018). Effects of Arousal on Mouse Sensory Cortex Depend on Modality. Cell Rep. *22*, 3160–3167. https://doi.org/10.1016/j.celrep.2018.02.092.
28. Fu, Y., Tucciarone, J.M., Espinosa, J.S., Sheng, N., Darcy, D.P., Nicoll, R.A., Huang, Z.J., and Stryker, M.P. (2014). A Cortical Circuit for Gain Control by Behavioral State. Cell *156*, 1139–1152. https://doi.org/10.1016/j.cell.2014.01.050.
29. Bimbard, C., Sit, T.P.H., Lebedeva, A., Reddy, C.B., Harris, K.D., and Carandini, M. (2023). Behavioral origin of sound-evoked activity in mouse visual cortex. Nat. Neurosci. *26*, 251–258. https://doi.org/10.1038/s41593-022-01227-x.
30. Vinck, M., Batista-Brito, R., Knoblich, U., and Cardin, J.A. (2015). Arousal and Locomotion Make Distinct Contributions to Cortical Activity Patterns and Visual Encoding. Neuron *86*, 740–754. https://doi.org/10.1016/j.neuron.2015.03.028.
31. McGinley, M.J., David, S.V., and McCormick, D.A. (2015). Cortical Membrane Potential Signature of Optimal States for Sensory Signal Detection. Neuron *87*, 179–192. https://doi.org/10.1016/j.neuron.2015.05.038.
32. Bennett, C., Arroyo, S., and Hestrin, S. (2013). Subthreshold Mechanisms Underlying State-Dependent Modulation of Visual Responses. Neuron *80*, 350–357. https://doi.org/10.1016/j.neuron.2013.08.007.
33. Niell, C.M., and Stryker, M.P. (2010). Modulation of Visual Responses by Behavioral State in Mouse Visual Cortex. Neuron *65*, 472–479. https://doi.org/10.1016/j.neuron.2010.01.033.
34. Reimer, J., Froudarakis, E., Cadwell, C.R., Yatsenko, D., Denfield, G.H., and Tolias, A.S. (2014). Pupil Fluctuations Track Fast Switching of Cortical States during Quiet Wakefulness. Neuron *84*, 355–362. https://doi.org/10.1016/j.neuron.2014.09.033.
35. Welle, C.G., and Contreras, D. (2016). Sensory-driven and spontaneous gamma oscillations engage distinct cortical circuitry. J. Neurophysiol. *115*, 1821–1835. https://doi.org/10.1152/jn.00137.2015.
36. Kum, J.E., Han, H.-B., and Choi, J.H. (2016). Pupil Size in Relation to Cortical States during Isoflurane Anesthesia. Exp. Neurobiol. *25*, 86–92. https://doi.org/10.5607/en.2016.25.2.86.
37. Zehendner, C.M., Luhmann, H.J., and Yang, J.-W. (2013). A Simple and Novel Method to Monitor Breathing and Heart Rate in Awake and Urethane-Anesthetized Newborn Rodents. PLoS One *8*, e62628. https://doi.org/10.1371/journal.pone.0062628.
38. Tort, A.B.L., Brankačk, J., and Draguhn, A. (2018). Respiration-Entrained Brain Rhythms Are Global but Often Overlooked. Trends Neurosci. *41*, 186–197. https://doi.org/10.1016/j.tins.2018.01.007.
39. Cavelli, M., Castro-Zaballa, S., Gonzalez, J., Rojas-Líbano, D., Rubido, N., Velásquez, N., and Torterolo, P. (2020). Nasal respiration entrains neocortical long-range gamma coherence during wakefulness. Eur. J. Neurosci. *51*, 1463–1477. https://doi.org/10.1111/ejn.14560.
40. González, J., Cavelli, M., Mondino, A., Castro-Zaballa, S., Brankačk, J., Draguhn, A., Torterolo, P., and Tort, A.B.L. (2023). Breathing modulates gamma synchronization across species. Pflugers Arch. *475*, 49–63. https://doi.org/10.1007/s00424-022-02753-0.
41. Ito, J., Roy, S., Liu, Y., Cao, Y., Fletcher, M., Lu, L., Boughter, J.D., Grün, S., and Heck, D.H. (2014). Whisker barrel cortex delta oscillations and gamma power in the awake mouse are linked to respiration. Nat. Commun. *5*, 3572. https://doi.org/10.1038/ncomms4572.
42. Rojas-Líbano, D., Wimmer Del Solar, J., Aguilar-Rivera, M., Montefusco-Siegmund, R., and Maldonado, P.E. (2018). Local cortical activity of distant brain areas can phase-lock to the olfactory bulb's respiratory rhythm in the freely behaving rat. J. Neurophysiol. *120*, 960–972. https://doi.org/10.1152/jn.00088.2018.
43. Zhong, W., Ciatipis, M., Wolfenstetter, T., Jessberger, J., Müller, C., Ponsel, S., Yanovsky, Y., Brankačk, J., Tort, A.B.L., and

Draguhn, A. (2017). Selective entrainment of gamma subbands by different slow network oscillations. Proc. Natl. Acad. Sci. USA *114*, 4519–4524. https://doi.org/10.1073/pnas.1617249114.

44. Tort, A.B.L., Komorowski, R., Eichenbaum, H., and Kopell, N. (2010). Measuring Phase-Amplitude Coupling Between Neuronal Oscillations of Different Frequencies. J. Neurophysiol. *104*, 1195–1210. https://doi.org/10.1152/jn.00106.2010.
45. Meneghetti, N., Cerri, C., Tantillo, E., Vannini, E., Caleo, M., and Mazzoni, A. (2021). Narrow and Broad gamma Bands Process Complementary Visual Information in Mouse Primary Visual Cortex. eNeuro *8*, ENEURO.0106-21.2021. https://doi.org/10.1523/ENEURO.0106-21.2021.
46. Saleem, A.B., Lien, A.D., Krumin, M., Haider, B., Rosón, M.R., Ayaz, A., Reinhold, K., Busse, L., Carandini, M., and Harris, K.D. (2017). Subcortical Source and Modulation of the Narrowband Gamma Oscillation in Mouse Visual Cortex. Neuron *93*, 315–322. https://doi.org/10.1016/j.neuron.2016.12.028.
47. Shin, D., Peelman, K., Lien, A.D., Del Rosario, J., and Haider, B. (2023). Narrowband gamma oscillations propagate and synchronize throughout the mouse thalamocortical visual system. Neuron *111*, 1076–1085.e8. https://doi.org/10.1016/j.neuron.2023.03.006.
48. Lohuis, M.N.O., Marchesi, P., Olcese, U., and Pennartz, C. (2022). Triple dissociation of visual, auditory and motor processing in primary visual cortex. Preprint at bioRxiv. https://doi.org/10.1101/2022.06.29.498156.
49. Carter, M.E., Yizhar, O., Chikahisa, S., Nguyen, H., Adamantidis, A., Nishino, S., Deisseroth, K., and De Lecea, L. (2010). Tuning arousal with optogenetic modulation of locus coeruleus neurons. Nat. Neurosci. *13*, 1526–1533. https://doi.org/10.1038/nn.2682.
50. Poe, G.R., Foote, S., Eschenko, O., Johansen, J.P., Bouret, S., Aston-Jones, G., Harley, C.W., Manahan-Vaughan, D., Weinshenker, D., Valentino, R., et al. (2020). Locus coeruleus: a new look at the blue spot. Nat. Rev. Neurosci. *21*, 644–659. https://doi.org/10.1038/s41583-020-0360-9.
51. Reimer, J., McGinley, M.J., Liu, Y., Rodenkirch, C., Wang, Q., McCormick, D.A., and Tolias, A.S. (2016). Pupil fluctuations track rapid changes in adrenergic and cholinergic activity in cortex. Nat. Commun. *7*, 13289. https://doi.org/10.1038/ncomms13289.
52. Hilaire, G., Viemari, J.-C., Coulon, P., Simonneau, M., and Bévengut, M. (2004). Modulation of the respiratory rhythm generator by the pontine noradrenergic A5 and A6 groups in rodents. Respir. Physiol. Neurobiol. *143*, 187–197. https://doi.org/10.1016/j.resp.2004.04.016.
53. Kim, T., Thankachan, S., McKenna, J.T., McNally, J.M., Yang, C., Choi, J.H., Chen, L., Kocsis, B., Deisseroth, K., Strecker, R.E., et al. (2015). Cortically projecting basal forebrain parvalbumin neurons regulate cortical gamma band oscillations. Proc. Natl. Acad. Sci. USA *112*, 3535–3540. https://doi.org/10.1073/pnas.1413625112.
54. McNally, J.M., Aguilar, D.D., Katsuki, F., Radzik, L.K., Schiffino, F.L., Uygun, D.S., McKenna, J.T., Strecker, R.E., Deisseroth, K., Spencer, K.M., and Brown, R.E. (2021). Optogenetic manipulation of an ascending arousal system tunes cortical broadband gamma power and reveals functional deficits relevant to schizophrenia. Mol. Psychiatry *26*, 3461–3475. https://doi.org/10.1038/s41380-020-0840-3.
55. Neves, R.M., Van Keulen, S., Yang, M., Logothetis, N.K., and Eschenko, O. (2018). Locus coeruleus phasic discharge is essential for stimulus-induced gamma oscillations in the prefrontal cortex. J. Neurophysiol. *119*, 904–920. https://doi.org/10.1152/jn.00552.2017.
56. Brunet, N.M., Bosman, C.A., Vinck, M., Roberts, M., Oostenveld, R., Desimone, R., De Weerd, P., and Fries, P. (2014). Stimulus repetition modulates gamma-band synchronization in primate visual cortex. Proc. Natl. Acad. Sci. USA *111*, 3626–3631. https://doi.org/10.1073/pnas.1309714111.
57. Allen, A.E., Procyk, C.A., Brown, T.M., and Lucas, R.J. (2017). Convergence of visual and whisker responses in the primary somatosensory thalamus (ventral posterior medial region) of the mouse: Visual responses in the somatosensory thalamus. J. Physiol. *595*, 865–881. https://doi.org/10.1113/JP272791.
58. Bieler, M., Xu, X., Marquardt, A., and Hanganu-Opatz, I.L. (2018). Multisensory integration in rodent tactile but not visual thalamus. Sci. Rep. *8*, 15684. https://doi.org/10.1038/s41598-018-33815-y.
59. Komura, Y., Tamura, R., Uwano, T., Nishijo, H., and Ono, T. (2005). Auditory thalamus integrates visual inputs into behavioral gains. Nat. Neurosci. *8*, 1203–1209. https://doi.org/10.1038/nn1528.
60. Noesselt, T., Tyll, S., Boehler, C.N., Budinger, E., Heinze, H.-J., and Driver, J. (2010). Sound-Induced Enhancement of Low-Intensity Vision: Multisensory Influences on Human Sensory-Specific Cortices and Thalamic Bodies Relate to Perceptual Enhancement of Visual Detection Sensitivity. J. Neurosci. *30*, 13609–13623. https://doi.org/10.1523/JNEUROSCI.4524-09.2010.
61. McBurney-Lin, J., Lu, J., Zuo, Y., and Yang, H. (2019). Locus coeruleus-norepinephrine modulation of sensory processing and perception: A focused review. Neurosci. Biobehav. Rev. *105*, 190–199. https://doi.org/10.1016/j.neubiorev.2019.06.009.
62. Molnár, B., Sere, P., Bordé, S., Koós, K., Zsigri, N., Horváth, P., and Lőrincz, M.L. (2021). Cell Type-Specific Arousal-Dependent Modulation of Thalamic Activity in the Lateral Geniculate Nucleus. Cereb. Cortex Commun. *2*, tgab020. https://doi.org/10.1093/texcom/tgab020.
63. Schneider, M., Broggini, A.C., Dann, B., Tzanou, A., Uran, C., Sheshadri, S., Scherberger, H., and Vinck, M. (2021). A mechanism for inter-areal coherence through communication based on connectivity and oscillatory power. Neuron *109*, 4050–4067.e12. https://doi.org/10.1016/j.neuron.2021.09.037.
64. Liang, L., Fratzl, A., Reggiani, J.D.S., El Mansour, O., Chen, C., and Andermann, M.L. (2020). Retinal Inputs to the Thalamus Are Selectively Gated by Arousal. Curr. Biol. *30*, 3923–3934.e9. https://doi.org/10.1016/j.cub.2020.07.065.
65. Schröder, S., Steinmetz, N.A., Krumin, M., Pachitariu, M., Rizzi, M., Lagnado, L., Harris, K.D., and Carandini, M. (2020). Arousal Modulates Retinal Output. Neuron *107*, 487–495.e9. https://doi.org/10.1016/j.neuron.2020.04.026.
66. Lohse, M., Dahmen, J.C., Bajo, V.M., and King, A.J. (2021). Subcortical circuits mediate communication between primary sensory cortical areas in mice. Nat. Commun. *12*, 3916. https://doi.org/10.1038/s41467-021-24200-x.
67. Koepsell, K., Wang, X., Vaingankar, V., Wei, Y., Wang, Q., Rathbun, D.L., Usrey, W.M., Hirsch, J.A., and Sommer, F.T. (2009). Retinal oscillations carry visual information to cortex. Front. Syst. Neurosci. *3*, 4. https://doi.org/10.3389/neuro.06.004.2009.
68. Storchi, R., Bedford, R.A., Martial, F.P., Allen, A.E., Wynne, J., Montemurro, M.A., Petersen, R.S., and Lucas, R.J. (2017). Modulation of Fast Narrowband Oscillations in the Mouse Retina and dLGN According to Background Light Intensity. Neuron *93*, 299–307. https://doi.org/10.1016/j.neuron.2016.12.027.
69. Spacek, M.A., Crombie, D., Bauer, Y., Born, G., Liu, X., Katzner, S., and Busse, L. (2022). Robust effects of corticothalamic feedback and behavioral state on movie responses in mouse dLGN. Elife *11*, e70469. https://doi.org/10.7554/eLife.70469.
70. Lewis, L.D., Voigts, J., Flores, F.J., Schmitt, L.I., Wilson, M.A., Halassa, M.M., and Brown, E.N. (2015). Thalamic reticular nucleus induces fast and local modulation of arousal state. Elife *4*, e08760. https://doi.org/10.7554/eLife.08760.
71. Campbell, P.W., Govindaiah, G., Masterson, S.P., Bickford, M.E., and Guido, W. (2020). Synaptic properties of the feedback connections from the thalamic reticular nucleus to the dorsal lateral geniculate nucleus. J. Neurophysiol. *124*, 404–417. https://doi.org/10.1152/jn.00757.2019.
72. Halassa, M.M., Chen, Z., Wimmer, R.D., Brunetti, P.M., Zhao, S., Zikopoulos, B., Wang, F., Brown, E.N., and Wilson, M.A. (2014). State-Dependent Architecture of Thalamic Reticular Subnetworks. Cell *158*, 808–821. https://doi.org/10.1016/j.cell.2014.06.025.
73. Hoseini, M.S., Higashikubo, B., Cho, F.S., Chang, A.H., Clemente-Perez, A., Lew, I., Ciesielska, A., Stryker, M.P., and Paz, J.T. (2021). Gamma rhythms and visual information in mouse V1 specifically modulated by somatostatin+ neurons in reticular thalamus. Elife *10*, e61437. https://doi.org/10.7554/eLife.61437.
74. Juventin, M., Zbili, M., Fourcaud-Trocmé, N., Garcia, S., Buonviso, N., and Amat, C. (2023). Respiratory rhythm modulates membrane potential and spiking of non-olfactory neurons. J. Neurophysiol. *130*, 1552–1566. https://doi.org/10.1152/jn.00487.2022.
75. Yackle, K., Schwarz, L.A., Kam, K., Sorokin, J.M., Huguenard, J.R., Feldman, J.L., Luo, L., and Krasnow, M.A. (2017). Breathing control center neurons that promote arousal in mice. Science *355*, 1411–1415. https://doi.org/10.1126/science.aai7984.
76. Harris, K.D., and Thiele, A. (2011). Cortical state and attention. Nat. Rev. Neurosci. *12*, 509–523. https://doi.org/10.1038/nrn3084.
77. Clement, E.A., Richard, A., Thwaites, M., Ailon, J., Peters, S., and Dickson, C.T. (2008). Cyclic and Sleep-Like Spontaneous Alternations of Brain State Under Urethane Anaesthesia. PLoS One *3*, e2004. https://doi.org/10.1371/journal.pone.0002004.
78. Reppas, J.B., Usrey, W.M., and Reid, R.C. (2002). Saccadic Eye Movements Modulate Visual Responses in the Lateral Geniculate Nucleus. Neuron *35*, 961–974. https://doi.org/10.1016/S0896-6273(02)00823-1.

79. Román Rosón, M., Bauer, Y., Kotkat, A.H., Berens, P., Euler, T., and Busse, L. (2019). Mouse dLGN Receives Functional Input from a Diverse Population of Retinal Ganglion Cells with Limited Convergence. Neuron *102*, 462–476.e8. https://doi.org/10.1016/j.neuron.2019.01.040.

80. Piscopo, D.M., El-Danaf, R.N., Huberman, A.D., and Niell, C.M. (2013). Diverse Visual Features Encoded in Mouse Lateral Geniculate Nucleus. J. Neurosci. *33*, 4642–4656. https://doi.org/10.1523/JNEUROSCI.5187-12.2013.

81. R Core Team (2020). R: A Language and Environment for Statistical Computing (R Foundation for Statistical Computing). https://www.R-project.org/.

82. Roesch, A., and Schmidbauer, H. (2018). WaveletComp: Computational Wavelet Analysis. R package version 1.1. https://CRAN.R-project.org/package=WaveletComp.

83. Cohen, M.X. (2014). Analyzing Neural Time Series Data: Theory and Practice, *Chapter 7* (MIT Press). https://doi.org/10.7551/mitpress/9609.001.0001.

STAR★METHODS

KEY RESOURCES TABLE

REAGENT or RESOURCE	SOURCE	IDENTIFIER
Chemicals, peptides, and recombinant proteins		
Urethane	Sigma-Aldrich	Cat#U2500; CAS: 51-79-6
Acepromazine	CP-Pharma	Cat#1227; CAS: 3598-37-6
Muscimol	Tocris Bioscience	Cat#0289; CAS: 2763-96-4
Experimental models: Organisms/strains		
Mouse/C57BL/6J	Charles River	Cat#632; RRID:IMSR_JAX:000664
Mouse/Ai32	Jackson Laboratories	RRID: IMSR_JAX: 012569
Mouse/Gad2-IRES-Cre	Jackson Laboratories	RRID: IMSR_JAX: 010802
Software and algorithms		
pClamp 8 / 11	Molecular Devices	https://www.moleculardevices.com/
R version 3.6.3 (2020-02-29)	R Core Team	https://cran.r-project.org/
Other		
Headstage	Digitimer	NL100AK
Preamplifier	Digitimer	NL104A
Digitizer	Molecular Devices	Axon Digidata 1320B / 1550B
Headstage	Molecular Devices	HS-2A
Amplifier	Molecular Devices	AxoClamp 2B
Fiber Optic Cannula	Thorlabs	CFM52L10

RESOURCE AVAILABILITY

Lead contact

Further information and requests for resources and reagents should be directed to and will be fulfilled by the lead contact, Clément E. Lemercier (clement.lemercier@rub.de).

Materials availability

This study did not generate new reagents.

Data and code availability

- All data reported in this paper will be shared by the lead contact upon request.
- This paper does not report original code.
- Any additional information required to reanalyze the data reported in this paper is available from the lead contact upon request.

EXPERIMENTAL MODEL AND STUDY PARTICIPANT DETAILS

Animals

Experimental procedures were conducted according to both European Union and German animal welfare regulations and were approved in advance by the local government's ethics committee (Landesamt für Arbeitsschutz, Naturschutz, Umweltschutz und Verbraucherschutz, Nordrhein-Westfalen, Germany). Experiments were performed on wild type C57BL/6J mice (Charles River, Sulzfeld, DE; Cat#632; RRID:IMSR_JAX:000664), of both sexes, aged 3-6 months. Animals were group-housed in ventilated cabinets on a 12-h reversed light/dark cycle. Food and water were provided *ad libitum*. Optogenetic experiments were carried on animals obtained through crossbreeding Ai32 (Jackson Laboratory, Bar Harbor, USA; RRID:IMSR_JAX:012569) and Gad2-IRES-cre (Jackson Laboratory; RRID:IMSR_JAX:010802) transgenic mice.

METHOD DETAILS

Surgical procedures

Mice were anesthetized by an intraperitoneal injection of a physiological saline mixture of urethane (1.2–1.4 g/kg, Sigma-Aldrich Chemie GmbH, Steinheim, Germany) and acepromazine (0.5 mg/kg, CP-Pharma Handelsgesellschaft mbH, Burgdorf, Germany). Body temperature

was maintained at 37°C with a closed loop heating pad (FHC Inc., Bowdoin, ME, USA), oxygen (≥ 99,5 %) was supplied continuously, and the animal's respiration rate was monitored on an oscilloscope through a piezoelectric transducer (27 mm diameter) positioned beneath its chest.[37] The scalp was locally anesthetized with bupivacaine (0.25 %, mibe GmbH Arzneimittel, Brehna, Germany), incised, and a custom head-fixation implant comprising an attachment point and a circular hole used as recording chamber was fixed onto the right hemisphere skull with dental acrylic (Paladur, Kulzer GmbH, Hanau, Germany). The skull was gently thinned to transparency with a dental drill (OS-40; Osada Electric Co., Ltd. Tokyo, Japan) and intrinsic optical signal imaging was then performed to functionally guide the craniotomies (~1 mm^2) over V1 and A1. In another set of experiments, a craniotomy of ~1 mm^2 was performed over the dorsolateral geniculate nucleus (dLGN), at 2.3 mm lateral and 2.5 mm posterior to bregma.[79]

Imaging of intrinsic optical signals

The setup intrinsic optical signal imaging comprised a data acquisition system (Imager 3001, Optical Imaging, Inc., Rehovot, Israel), a CCD camera (Adimec 1000m; Adimec, Eindhoven, Netherlands) and a 90 mm macro lens (Tamron Co. Ltd., Saitama, Japan). Image resolution was 1,000 x 1,000 pixels for a pixel size of ~10 μm. Illumination was generated by a halogen light source (Zeiss HAL 100; Carl Zeiss MicroImaging GmbH, Göttingen, Germany) under constant current supply, and was time-controlled with an optical shutter (Uniblitz VS14; Vincent Associates, Rochester, NY, USA). Images of the superficial blood vessel pattern were obtained by focusing the camera on the pial surface, while illuminating the cortex at 546 nm. For functional imaging, the illumination wavelength was switched to 630 nm, focus was adjusted ~400 μm below the brain surface, and prior to acquisition, light intensity was adjusted just below the camera's saturation level. Data acquisition started after 2 sec of initial illumination and comprised 1 sec of pre-stimulation, 1 sec of stimulation and 4 sec of post-stimulation recordings. Sensory stimuli and data acquisition were synchronized by establishing communication between the Imager 3001 system, the optical shutter, and the programmable pulse stimulator (Master-9). Raw images were acquired at a rate of 50 frames per second (fps) and then temporally binned to a rate of 5 fps. The change in reflectance relative to baseline was visualized as ΔR by calculating (R – R0), where 'R0' represents the average amount of light reflected prior start of the sensory stimulation, and 'R' represents the amount of light reflected during any given frame. To improve the signal-to-noise ratio, a minimum of 3 trials, with 20 sec intertrial intervals, were averaged. Cortical responses to sensory stimuli were visualized by using the WinMix 1.9 software (Optical imaging Inc.) after spatial binning (10×10) and clipping (generally 2-3 times the image standard deviation).

Sensory stimulation

Monocular visual stimulation was achieved using a light-emitting diode (LED, diameter: 5 mm, 572 nm, 20°, 16,000 mcd). The LED was controlled by a microcontroller (Arduino Uno Rev3; Arduino SRL, Monza, Italy). The LED was connected to a PVC-insulated polymethyl methacrylate (PMMA) optical fiber (outer diameter: 3.5 mm, inner diameter: 3 mm, length: 40 cm) and the tip of the optical fiber was placed ~1 cm from the animal's left eyeball. Visual stimulation consisted of a light flash of 1 sec (~100 lux, calibrated with TSL2561; Adafruit Industries, New York, NY, USA). Auditory stimuli were produced by a triggerable arbitrary waveform generator (Rigol DG811; Rigol Technologies, Inc., Portland, OR, USA), connected to a power amplifier (Nobsound AK170; bandwidth: 20 Hz - 20 kHz; Nobsound, Shenzhen Cavins Technology Co., Ltd., China) and a loudspeaker (FR 10 - 4 Ω; VISATON GmbH & Co. KG, Haan, Germany) placed at a distance of ~30 cm to the left of the animal's head. Auditory stimuli consisted of an open field white-noise burst, delivered at 80 dB SPL, unless otherwise specified (i.e., Figure 2; calibrated with Voltcraft SL-200; Conrad Electronic SE, Hirschau, Germany), using durations of either 1 sec, or 100 ms. The ambient noise level of room was ~45 dB SPL. Stimulators were triggered by a programmable pulse generator (Master-9; A.M.P. Instruments, Ltd., Jerusalem, Israel). All experiments were carried out in the dark.

Electrophysiological recordings

Intracortical local field potentials (LFPs) were recorded by means of ~1.5 MΩ borosilicate microelectrodes inserted in the layer 4 of V1 and A1 with the help of two separate stereotaxic micromanipulators (SM-25C; Narishige Scientific Instruments, Tokyo, Japan). Signals were amplified (NL100AK, NL104A; Digitimer Ltd., Welwyn Garden City, UK), high-pass filtered at 0.1 Hz, digitalized at 10 kHz (Axon Digidata 1550B; Molecular Devices, LLC. San Jose, CA, USA) and visualized with the pClamp 11 software (Molecular Devices).

Single-unit juxtacellular recordings of dLGN neurons were obtained using 2-3 MΩ borosilicate microelectrodes with the help of a motorized micromanipulator (SM-1; Luigs & Neumann GmbH, Ratingen, Germany). dLGN neurons were identified on an audiomonitor by their rapid spiking in response to either switching-on (dLGN-ON neurons) or switching-off (dLGN-OFF neurons) light flashes delivered at the contralateral visual field of the animal.[80] Neurons were recorded one by one along the gradual descent of the electrode. Signals were amplified (AxoClamp 2B; Molecular Devices), high pass filtered at 300 Hz, digitalized at 20 kHz (Axon Digidata 1320B; Molecular Devices), and visualized with the pClamp 8 software (Molecular Devices). For both cortical and thalamic recordings, glass microelectrodes were filled with an extracellular solution containing in mM:135 NaCl, 5.4 KCl, 1.8 $CaCl_2$, 1 $MgCl_2$, and 5 HEPES (pH ~7.2).

Ligand infusion

Activity of A1 (ipsilateral to V1 recording site) was silenced with an infusion of ~1 μL of the $GABA_A$-receptor agonist, muscimol (Tocris Bioscience, Wiesbaden-Nordenstadt, Germany), at a dose of 1 mM dissolved in extracellular solution. The mixture was loaded in the recording glass microelectrode and was ejected at the recording location (layer IV) by applying gentle positive pressure (Inverted suction-pulser; Sigmann

Elektronik GmbH, Hüffenhardt, German). To allow the mixture to flow out of the electrode, electrode tip was mechanically enlarged. As a result, the electrode resistance decreased ~1.5 to ~0.2 MΩ, and the auditory-evoked potentials showed reduced amplitudes compared to when recorded using standard electrodes.

Optogenetic stimulation

Experiments involving optogenetic manipulations were performed on transgenic mice that constitutively express channelrhodopsin selectively in all glutamate acid decarboxylase-2 (GAD2)-positive neurons (see Experimental model and study participant details section). Photostimulation of GAD2-expressing neurons via channelrhodopsin was achieved with 470 nm light pulses delivered by a fiber-coupled LED light source (M470F1; Thorlabs, Newton, NJ, USA). The optic fiber was positioned closely above the surface of A1 (ipsilateral to V1 recording site). The pulse length was 1.1 sec, starting 100 ms prior to sensory stimulation, with a light intensity ranging from 0.6 to 2.4 mW. The output power of the LED driver (DC2100; Thorlabs) was controlled by the voltage output of the programmable pulse stimulator (Master-9). The power output at the optic fiber cannula (CFM52L10; Thorlabs) tip was measured with a photodiode power sensor (PM100D; Thorlabs).

Imaging of the pupil

Images of the pupil were acquired under infrared illumination at 40 fps with the Raspberry Pi HQ camera module (no IR-cut filter; Raspberry Pi Foundation, Cambridge, UK) mounted on a 16 mm telephoto lens (CGL Electronics Co. Ltd., Hong Kong, China). A light flash, synchronized with sensory stimulation delivered outside the animal's visual field, enabled the epoching of the trials. Frames were cropped around the pupil (width: 160, height: 90 pixels) and extracted with the FFmpeg program. Pupil segmentation and tracking of its diameter were performed using the ImageJ software (NIH, Bethesda, MD, USA). Pupil imaging was conducted only in a subset of experiments and was not synchronized with electrophysiological measurements.

Monitoring of respiration and body movement

Animal respiration was monitored with a piezoelectric transducer (PZT; 27 mm diameter) placed beneath the animal's chest.[37] The PZT also enabled the detection of body movements. The raw signals from the PZT were digitalized at 10 kHz (Axon Digidata 1550B; Molecular Devices) in parallel with electrophysiological measurements. Monitoring of respiration were not systematically conducted in all experiments.

Recording protocol

Stimulus presentation was not randomized and was presented in a block fashion, with each block consisting of 20 repetitions with an inter-trial time interval of 10 seconds. LFPs were recorded in 6-second epochs, which included 1 second of pre-stimulation, 1 second of sensory stimulation, and 4 seconds of post-stimulation. In all experiments, audio-visual blocks were alternated with control blocks consisting of visual stimulation alone.

QUANTIFICATION AND STATISTICAL ANALYSIS

Data processing, analysis, visualization, and statistics were conducted using the R software.[81]

Quantification of sensory-evoked potentials

LFP time-series were down-sampled to 1 kHz with the R package *'gsignal'*. To ensure consistent quantification of sensory-evoked potential amplitude across trials, data were baseline-corrected by subtracting the mean voltage value from the 100 ms preceding sensory stimulation.

Spectral analysis of local field potentials

LFP time-series were down-sampled to 1 kHz and bandpass filtered between 0.1 to 300 Hz using a 2^{nd} order Butterworth bandpass filter, with the R package *'gsignal'*. The wavelet power spectrum of the filtered LFP time-series was obtained by applying a Morlet wavelet transform with the R package *'WaveletComp v.1.1'*.[82] The detection period range was set from 8 to 1024 ms, in which each octave was divided into 60 sub-octaves. V1 LFP time-series were divided into three different time periods: 1) A baseline period of 800 ms prior to stimulus onset containing the spontaneous LFP fluctuations; 2) A transient a period of 200 ms after stimulation onset, containing the initial event-related change in the LFP (i.e., visual-evoked potential); 3) A stimulation period ranging from 200 ms to 1 sec after stimulation onset, containing later event-related changes in the LFP (i.e., visually-driven oscillatory activity). The power increase (Δ Power) in the LFP during the stimulation period (stim) relative to the baseline period (base), was computed by subtracting the power spectral density (PSD) values of these two phases (Δ Power = $Power_{stim} - Power_{base}$). From these differential spectra, power, frequency, and bandwidth of the oscillations were quantified by measuring either their band power (40 to 80 Hz), peak frequency and half bandwidth (i.e., at 50% of peak power).

Analysis of single-unit activity

Spike detection was conducted using the threshold search function of the software pClamp 11 (Molecular Devices). Peristimulus time histograms (PSTHs) were determined with a bin size of 10 ms over 6-second epochs, which included 1 second of pre-stimulation, 1 second of sensory stimulation, and 4 seconds of post-stimulation. From these PSTHs, Kernel density estimation (R base package *'stats'*, with the 'bw'

argument of the 'density' function set to 1/50) was used to estimate the density of the PSTHs. Spike train power spectra were computed from binary spike train data with the R package *'psd'*. Change in spike rate (unless otherwise stated, i.e., Figures 6I and 6J) and power was evaluated between the 1-second baseline period immediately prior sensory stimulation, and the 1-second stimulation period in which sensory stimuli were delivered.

Spectral analysis of respiratory signals

PZT signals were down-sampled from 10 to 1 kHz with the R package *'gsignal'*, and wavelet power spectra were obtained by applying a Morlet wavelet transform with the R package *'WaveletComp v.1.1'*[82] with detection range set from 100 to 4096 ms, where each octave were divided into 60 suboctaves. Low-frequency edge artifacts resulting from wavelet time-frequency decomposition were attenuated using a 'reflection' approach.[83] Changes in animal's respiration amplitude and frequency in response to sensory stimuli were evaluated by quantifying the peak power and peak frequency. These measures were derived from PSDs calculated during two intervals: half a second before and one second during sensory stimulation.

Phase-amplitude coupling analysis

The V1 LFP time-series were down-sampled to 1 kHz, bandpass filtered between 40-80 Hz using a 4^{th} order Butterworth bandpass filter, and the gamma amplitude (envelope) was obtained from the Hilbert transform with the R package *'gsignal'*. Similarly, the respiration time-series were filtered between 1-8 Hz using a 4^{th} order Butterworth bandpass filter, and the phase angle was obtained from the Hilbert transform with the R package *'gsignal'*. Respiratory phase was then binned into 18 bins, and the mean normalized gamma amplitude was calculated within each bin.[44]

Statistics

Unless stated, data in the text are reported as M (IQR) or M [IQR]; where 'M' is the median and 'IQR' is the interquartile range. In the results section, 'N' corresponds to the number of animals and 'n' corresponds to the number of neurons. To report statistics in the text, visual, auditory, and audio-visual conditions are respectively abbreviated as V, A and AV. The analysis between the V and AV conditions was conducted using averaged values, representing the mean of 20 consecutive trials. In all statistical analyses (except for the Figure 4), the results from the AV trials block were systematically compared to the preceding V trials block. Differences between matched and unmatched measurements were respectively evaluated with the Wilcoxon signed-rank test (Figures 1, 2, 3, 6, and 7) and Wilcoxon-Mann-Whitney U test (Figures 4 and 8). A p-value < 0.05 was considered statistically significant. Strength and direction of monotonic association between two variables were assessed with the Spearman's rank correlation coefficient (Figures 3 and 7). An analysis of covariance (ANCOVA) was employed to assess differences in slopes or intercepts within linear regression models (Figure 3). Data were visualized with the R software *'base'* and *'ggplot2'* packages.